Further development of the UCLA Atmospheric General Circulation Model through a new PBL parameterization

I NDEX

Abstract

This thesis discusses the implementation of a new parameterization of planetary boundary layer (PBL) processes in the UCLA Atmospheric General Circulation Model (AGCM). As in the previous versions of the UCLA AGCM, a sigma-type vertical coordinate is used for the PBL, sharing a coordinate surface with the free atmosphere at the PBL top. This framework facilitates an explicit representation of processes concentrated near the PBL top, which is crucial especially for predicting PBL clouds. In the new PBL parameterization, we introduce multiple layers between PBL top and Earth's surface, allowing for explicit prediction of the vertical profiles of potential temperature, water mixing ratio and horizontal winds within the PBL. The surface fluxes are determined from an aerodynamic formula, in which a combination of the square root of the bulk turbulent kinetic energy (TKE) and the grid-scale surface wind are used to represent the velocity scale. With this formulation, the surface fluxes estimates are expected to be better than with the traditional methods, since the grid-scale wind can be weak while the convective mixing is strong. The PBL-top mass entrainment is explicitly computed with a formulation that also uses the bulk TKE.

AGCM simulations with the new formulation of PBL are analyzed with a focus on the seasonal and diurnal variations. The simulated seasonal cycle of stratocumulus over the eastern oceans is realistic, so are the diurnal cycles of the PBL depth and precipitation over land. The simulated fluxes of latent heat, momentum and short wave radiation at the ocean surface and baroclinic activity in the middle latitudes show significant improvements over the previous versions of the AGCM based on the single-layer PBL.

We analyze the behavior of the simulated PBL, the seasonal and diurnal cycles of variables related to the PBL in particular, and some basic aspects of the simulated general circulation. The simulated seasonal cycle of marine stratocumulus over the eastern oceans is realistic, so are the diurnal cycles of the PBL depth and stratocumulus over land. The simulated surface fluxes of latent heat, momentum and short wave radiation heating at ocean surface show significant improvements over previous versions of the AGCM. This is encouraging in view of the potential use of the new version in coupled simulations with Ocean General Circulation Models (OGCM).

1. Introduction

A general overview

Great part of atmospheric movements are quasi bidimensional, and therefore, although they present non linear interaction (and specially energy exchanges) between movement components of different wave lengths, they don't have turbulent processes in the usual sense that this term has in fluid mechanics. According to this term, turbulent processes are characterized by single directed energy cascades; components of the movements of greater wave length transmit power to those of lesser wave length. More specifically, there are larger vortexes that results either from dynamic instability related with velocity shear of the large scale flux or from convective instability. In turn, instability due to shear of these large vortex generate vortexes of smaller scale, which in turn generate others, while vorticity field becomes progressively more disorganized as we consider smaller vortexes. As counterpart of this behavior, if we have a strictly bidimensional, non-divergent flux in a closed domain, of non viscous fluid, punctual vorticity is conserved, and consequently it is also conserved enstrophy (which is defined as the squared vorticity divided by two), both locally and globally. Global conservation of enstrophy (which is a positive defined quantity) prevents single direction energy cascades to occur, which doesn't happen in three dimensional fluxes, in which punctual vorticity is not conserved and therefore neither punctual or global enstrophy. As a way of illustrating the substantial differences between behavior of three dimensional and two dimensional fluxes, we can mention a classical result: in case of three dimensional turbulence, Kolmogorov hypothesis for vortexes of length scales included in the so called inertial range lead to conclude through dimensional analysis that kinetic energy spectrum for this

range is proportional to the -5/3 power of wave number. For bidimensional flows with non linear interactions among their several components, if we make the hypothesis that transmition of power between these components depends on enstrophy we conclude that spectrum of kinetic energy is proportional to the -3 power of wave number. Actually most of atmospheric movements are predominantly quasi bidimensional, quasi uncompressible and with negligeable viscous effects, and in fact it is found that the lae with -3 exponent is very approximately valid for flows with planetary wave number 8 or less. (Charney 1971).

Despite relative preponderance of quasi bidimensional flows in the atmopsheric general circulation, this includes some tridimensional and turbulent movements that affects it in fundamental ways. Two examples are the development of convective clouds and the breaking of vertically propagating gravity waves. Another most important example of turbulent atmospheric motion is that of the planetary boundary layer, which is the focus of this thesis.

PBL processes are dominated by turbulent fluxes, which play key roles in determining the vertical structure and the momentum and energy balances of the entire atmosphere through redistributing momentum heat and moisture from Earth's surface. The exchanges of mass, energy, moisture and momentum with the free atmosphere, on the other hand, affect the structure of the PBL, so that PBL processes influence climate through two-way interactions. An important example of such interactions appears through the occurrence of stratocumulus clouds in the PBL. The effect of this type of clouds on radiation is one of the most important components in the heat balance of the climatic system, while radiative cooling at the top of stratocumulus clouds becomes the primary

source of turbulence within the PBL. An appropriate simulation of this type of clouds is of great importance for the prediction of SSTs by coupled Atmosphere-Ocean models (Ma et al. 1996, Mechoso et al. 2000). Atmospheric general circulation models (AGCMs), however, generally do not have a sufficient resolution to resolve the detailed structure of PBL processes and, therefore, a parametric representation (parameterization) is needed.

Governing equations of AGCMs: Hydrostatic system of equations

The equations of momentum, mass continuity, first principle of thermodynamic, state and the water vapor and liquid vapor conservation, complemented with equation of state for ideal gases, make a complete system of prognostic equations for atmospheric motions. However, they include solutions of a very wide range of frequencies, including sound waves. It would be desirable an approximation that excludes waves of such elevated frequency and phase velocity, since in geophysics fluid dynamics we are not interested in such processes, while if the equation to be numerically integrated includes them, temporal discretization must sample them appropriately so the numerical system is linearly stable, which would result in an exaggerated computational cost. One of the approximations that is usually done in atmospheric models and excludes (filters) the sound waves is the hydrostatic approximation, in which the vertical component of acceleration is neglected respect to gravity, and the vertical momentum equation is taken as

$$g\delta z = -\frac{1}{\rho}\delta p$$

were the differential increments δ are taken for constant (x, y,t). Note that we don't have anymore a prognostic equation for the vertical component of the velocity, w, which has to

be diagnosed from the mass continuity equation. Methodology for integration is usually formulated in terms of sigma coordinate in pressure, and is discussed in detail in notes of Axxx course or in the BID CONICYT 117 report.

Governing equation of turbulent motion: Bousinesq and anelastic system of equations

The hydrostatic approximation filters several solution of superior frequency, but since it's based on neglecting vertical acceleration respect to gravity, it is not appropriate for the study of convective or turbulent processes, where vertical component of acceleration is not neglectable. For those cases, we can consider the anelastic Bousinesq approximation, which we outline in very general aspects here. We can find a detailed discussion on this approximation in Stull (1988).

We define a basic state of the virtual temperature, pressure and density fields that verify the hydrostatic relation, we call the fields of this basic state T_{vo} (o θ_{vo}), ρ_o, p_o. If ψ is any of these variables, we define $\delta\psi$ as its departure from the basic state,

$$\delta\psi \equiv \psi - \psi_0$$

applying equation of state to the $\psi+\psi_0=\delta\psi$ variables, and neglecting those term which are of second order in the perturbations, we can get the following approximate relationship:

$$\frac{\delta p}{p_0} = \frac{\delta T_v}{T_{v0}} + \frac{\delta \rho}{\rho_0}.$$

Since in a vertical displacement of a fluid parcel this tend to acquire the pressure of the unperturbed environment in its new height, which means $\delta p \approx 0$, while its temperature and density vary according to the law of an adiabatic expansion form the initial to the new pressure, we can consider that $\delta p/p_0 << \delta T/T_0$ and $\delta p/p_0 << \delta\rho/\rho_0$, so we can write the following approximation:

$$\frac{\delta T_v}{T_{v0}} \approx -\frac{\delta \rho}{\rho_0}. \qquad (1.1a)$$

We can also show, by writing $\delta\theta_v$ as function of δT_v y δp (through a first order Taylor development of the definition of θv[1]),

$$\frac{\delta \theta_v}{\theta_{v0}} \approx -\frac{\delta \rho}{\rho_0} \qquad (1.1b)$$

Applying this approximation, and others consistent with this, we obtain a prognostic set for equations with anelastic approximation. In this introduction we would like only to show vertical component of momentum equation, since it is of particular significance.

$$\frac{dw}{dt} = -g\frac{dq_v}{q_{vo}} + u\nabla^2 w$$

The first term at the right hand side of this equation deserves physical interpretation. We can consider that convective turbulence in the PBL implies upward and downward displacements of fluid parcels that otherwise would be in a hydrostatic balance. Lets suppose that a parcel is very close to the ground, with a potential virtual temperature θ_{v1}, and it rises to certain height, were the environment is at a potential virtual temperature θ_{v2}, which we suppose for the purposes of this example lesser than θ_{v1}. In its vertical displacement the parcel conserves its original potential virtual temperature θ_{v1}, and then $\delta\theta_v = \theta_{v1} - \theta_{v2}$. Since $\theta_{v1} > \theta_{v2}$, and we also suppose that the parcel is at the unperturbed pressure of the environment ($\delta p = 0$), the parcel will be lighter than the environment, and thus will tend to continue its rise. In the basic state, the force per unit of mass associated with the pressure gradient force is equilibrated with the weight of any generic parcel, but

[1] $q \equiv T\left(p_{ref.}/p\right)^{R/c_P}$, potential temperature, conserved in adiabatic processes. Usually p_{ref}=1000hPa. θ_v is defined analogously with T_v.

that is not the case of the displaced parcel of the example. The term $g\delta\theta_v/\theta_{v0}$ is associated with the Archimedes buoyancy, per unit of mass, that is, vertical pressure gradient force fraction that is not compensated by the parcel weight, since this is smaller. We shall find bellow that positive values of $\delta\theta_v$ associated with upward displacements (or negative associated with downward displacements) are associated with creation of turbulent kinetic energy, while the opposite situation is associated with its destruction.

We would like to make an additional comment about the anelastic approximation: since we consider the relative pressure perturbations of lesser order than the relative perturbations of density and temperature, while we balance the former two in the state equation, we are excluding those processes in which the pressure increases associated with the gas compression play a relevant role (and so the "anelastic" name). This makes more natural to expect the fact that the equations obtained with the anelastic approximation filter the sound waves.

Equations for mean quantities in a turbulent flow

Atmospheric general circulation models usually solve motions of relative large scale, which are considered to fulfill the hydrostatic approximation. PBL turbulence is considered as a high frequency perturbation of this hydrostatic basic state, which in turn follows anelastic approximation. We make the hypothesis of frequency separation between these components of motion (the one explicitely solved by the AGCM and the turbulent one, whose effects have to be parameterized), which allows for classic Reynolds time averages technique. In the case of PBL studies, specially for the scales of motion solved by AGCMs, is common to consider only turbulent fluxes in the vertical direction. Considering this simplification, Reynolds equations of a large scale flow in

hydrostatic balance with turbulent perturbations that allow for anelastic approximation result in the following (see Stull 1988 for detailed deduction):

$$\frac{\partial \bar{u}}{\partial t} = -\bar{u}_j \frac{\partial \bar{u}}{\partial x_j} - \frac{\partial \overline{w'u'}}{\partial z} - \frac{1}{\bar{r}} \frac{\partial \bar{p}}{\partial x} - f\bar{v} \qquad (1.2a)$$

$$\frac{\partial \bar{v}}{\partial t} = -\bar{u}_j \frac{\partial \bar{v}}{\partial x_j} - \frac{\partial \overline{w'v'}}{\partial z} - \frac{1}{\bar{r}} \frac{\partial \bar{p}}{\partial y} + f\bar{u} \qquad (1.2b)$$

$$\frac{\partial \bar{q}}{\partial t} = -\bar{u}_j \frac{\partial \bar{q}}{\partial x_j} - \frac{\partial \overline{w'q}}{\partial z} + \frac{\bar{q}}{c_P T} Q \qquad (1.2c)$$

$$\frac{\partial \bar{q}}{\partial t} = -\bar{u}_j \frac{\partial \bar{q}}{\partial x_j} - \frac{\partial \overline{w'q'}}{\partial z} + S \qquad (1.2d)$$

Here q is the water vapor content, f. The rest of the symbols have their usual meanings. Advections are written with vector notation.

Equations for perturbations in a turbulent flow: turbulent fluxes and variances

We can also obtain equations for perturbations:

$$\frac{\partial u'}{\partial t} + \vec{V}'.\nabla u' + \vec{\bar{V}}.\nabla u' + \vec{V}'.\nabla \bar{u} + \nabla.\left(\overline{\vec{V}'u'}\right) = -\frac{1}{r}\frac{\partial p'}{\partial x} + u\nabla^2 u'$$

$$\frac{\partial v'}{\partial t} + \vec{V}'.\nabla v' + \vec{\bar{V}}.\nabla v' + \vec{V}'.\nabla \bar{v} + \nabla.\left(\overline{\vec{V}'v'}\right) = -\frac{1}{r}\frac{\partial p'}{\partial y} + u\nabla^2 v'$$

$$\frac{\partial w'}{\partial t} + \vec{V}'.\nabla u' + \vec{\bar{V}}.\nabla u' + \vec{V}'.\nabla \bar{u} + \nabla.\left(\overline{\vec{V}'u'}\right) = -\frac{1}{r}\frac{\partial p'}{\partial z} - g\left(1 - \frac{q'}{\bar{q}}\right) + u\nabla^2 w$$

(1.3) (equations for theta and q perturbation still to be added)

Equations (1.3) allow in turn (by multiplying them by w' and taking Reynolds time averages), to obtain predictio n equations for the vertical turbulent fluxes that appear in the right hand size of equations 1.2. In a similar way prediction equations for the variances of u', v' and w' (that is u'2, v'2, w'2) can be obtained, that in turn give,

through addition, a prediction equation for turbulent kinetic energy, defined as $e \equiv \left(\overline{u'^2 + v'^2 + w'^2}\right)/2$. Prediction equations for turbulent fluxes are (see Stull 1988) :

$$\frac{\partial \overline{w'u'}}{\partial t} = -\overline{w'^2}\frac{\partial \bar{u}}{\partial z} - \frac{\partial \overline{w'w'u'}}{\partial z} + g\frac{\overline{u'q_v'}}{\bar{q}_v} + \overline{\frac{p'}{\bar{r}}\left(\frac{\partial u'}{\partial z} + \frac{\partial w'}{\partial x}\right)} - 2e_{uw} \qquad (1.4a)$$

$$\frac{\partial \overline{w'v'}}{\partial t} = -\overline{w'^2}\frac{\partial \bar{v}}{\partial z} - \frac{\partial \overline{w'w'v'}}{\partial z} + g\frac{\overline{v'q_v'}}{\bar{q}_v} + \overline{\frac{p'}{\bar{r}}\left(\frac{\partial v'}{\partial z} + \frac{\partial w'}{\partial y}\right)} - 2e_{vw} \qquad (1.4b$$

$$\frac{\partial \overline{w'q'}}{\partial t} = -\overline{w'^2}\frac{\partial \bar{q}}{\partial z} - \frac{\partial \overline{w'w'q'}}{\partial z} + g\frac{\overline{q'q_v'}}{\bar{q}_v} + \frac{\overline{p'}}{\bar{r}}\frac{\partial \overline{q'}}{\partial z} - 2e_{qw} \qquad (1.4c)$$

$$\frac{\partial \overline{w'q'}}{\partial t} = -\overline{w'^2}\frac{\partial \bar{q}}{\partial z} - \frac{\partial \overline{w'w'q'}}{\partial z} + g\frac{\overline{q'q_v'}}{\bar{q}_v} + \frac{\overline{p'}}{\bar{r}}\frac{\partial \overline{q'}}{\partial z} - 2e_{qw} \qquad (1.4d)$$

while prognostic equation for e is

$$\frac{\partial e}{\partial t} = k\frac{r\overline{w's_v'}}{p}rg + \overline{w'u'}\frac{\partial u}{\partial z} + \overline{w'v'}\frac{\partial v}{\partial z} - \frac{1}{r}\frac{\partial}{\partial z}\left(r\overline{w'e'} + \overline{w'p'}\right) - e \qquad (1.5)$$

If direct use of equations (1.2) were possible, they would be used for predicting $\overline{w'u'}$, $\overline{w'v'}$, $\overline{w'\theta'}$ and $\overline{w'q'}$, which in term would allow for closure of equations (1.1) for $\bar{u}$, $\bar{v}$, $\bar{\theta}_v$ and $\bar{q}$. However this is not directly possible because we don't have relations for computing some of the terms at the right side of equations (1.2), as the triple products in (2.20a). However, for certain types of flows there are semi empirical relations that associate these undetermined terms with variables that do have prognostic or diagnostic equations. This originates the turbulence models for the Reynolds equations, which we discuss briefly below.

TKE prediction equation also requires additional closure assumptions. Nevertheless, TKE equation helps to understand the physical processes that originate the turbulence in

the PBL. Term $\overline{w'\theta'_v}g/\theta_v$ represents turbulent kinetic energy generation due to convective instability if its positive, or its destruction due to static stability if its negative. $\overline{w'\theta'_v}$ can be computed from $\overline{w'\theta'}$ and $\overline{w'q'}$ as will be shown bellow. Note that $\overline{w'\theta'}$ y $\overline{w'q'}$ also appear in the prognostic equations of $\bar{\theta}$ y $\bar{q}$ respectively, so they are of great importance in the PBL functioning. Terms $\overline{w'u'}\partial u/\partial z$ y $\overline{w'v'}\partial v/\partial z$ represent turbulent kinetic energy creation due to vertical shear of the horizontal velocity, that is also of great importance for all the boundary layers and in particular for the PBL. Term $1/\rho \times \partial\left(\overline{\rho w' e'} + \overline{w' p'}\right)/\partial z$ combines turbulent kinetic energy transport due to the turbulent motion and the contribution of the pressure power to this local balance of $\partial e/\partial t$. The effect of this term is to make more isotropic the statistical properties of the turbulence, a discussion about this can be found in Tenekes y Lumley (1972).

Simplification of equations and their application to the PBL

The equations discussed above are complicated and require proper closure assumptions to be applied to a model. Here we will discuss the simplification of the equations and their application to the PBL. First we briefly review the behavior and structure of the PBL in the next section.

PBL regimes and structure.

It is usually considered than in the first meters above the earths surface the vertical turbulent fluxes of horizontal velocity (and horizontal momentum), potential temperature and moisture can be considered constant respect to the vertical direction. This region is defined as *surface layer*, and through dimensional analysis we can determine the existence of universal functions that allows to compute the turbulent fluxes from information about the structure of this layer and the conditions of the Earth's surface. The

remain of the PBL is called *outer boundary layer*, and its structure depends fundamentally on which is the physical processes that generate the turbulence. As we saw, it can be generated either through wind shear or convective instability. The situation of convective instability can occur if the Earth's surface is at greater temperature than the ar above it, or ehen the PBL is topped by clouds, which implies radiative cooling at the PBL top. When one of these conditions occur, or both the PBL is called "convectively unstable", and the outer PBL is called also "mixed layer", within the mixed layer the convective eddies tend to produce a near statically neutral vertical profile. If there is no condensation, this implies $\partial\overline{\theta_v}/\partial z \approx 0$ (see, for example, Holton). We also will have a vertical profile of water vapor mixing ratio nearly homogeneous, $\partial\bar{q}/\partial z = 0$. It can be proof that the condition $\partial\overline{\theta_v}/\partial z = 0$ is approximately equivalent to $\partial\overline{s_v}/\partial z \approx 0$, where

$$s_v \equiv c_p T_v + gz \tag{1.6}$$

is the dry static energy. In case that condensation occurs within the PBL, there are also conditions of near neutral static energy, which now are expressed in terms of

$$h_v \equiv c_p T_v + gz + Lq \tag{1.7}$$

(L is the latent heat per unit of mass of water, 2.52x106 J/kg) and of r, total water mixing ratio, defined as $r \equiv q + l$, were l is the liquid water mixing ratio. The conditions of neutral stability are $\partial\overline{h_v}/\partial z = 0$ and $\partial\bar{r}/\partial z = 0$. A very important aspect of the convective PBL, is that since s_v (or h_v) is approximately vertically well mixed, while it grows with height in the free atmosphere, we usually have at the top of the PBL a thermal inversion, that is, temperature increases a few degrees with the vertical in a few meters. This inversion, as is convectively very stable, provides a well defined limit to the turbulence and hence to the PBL.

For the case when the Earth's surface is colder than the air above it, and there are not clouds, term $\overline{w'\theta_v'}g/\theta_v$ of equation 1.5 is negative, and eliminates turbulence, so it only can be generated by wind shear. This regime is called *stable PBL*, there is a thermal inversion immediately above the Earth's surface, and mixing in the outer PBL is not due to convective eddies, but due to the eddies generated by wind shear, which are of smaller scale. Outer PBL is now not neutral, and the vertical profile of θv is not necessarily homogeneous, but tend it grows with height, although due to the turbulent mixing it can have a growth with height lesser than that of the free atmosphere above. The thermal inversion at the PBL top will be more moderate than in the convectively unstable case, or will not occur at all, an the transition from a turbulent regime to the turbulent free atmosphere will span a greater vertical thickness. On the other hand, if there are condition of static stability and null wind, turbulence will be very weak or not occur at all.

Turbulence models for the PBL

Equations 1.4 might be considered as prognostic equations for $\overline{w'u'}$, $\overline{w'v'}$, $\overline{w'\theta'}$ and $\overline{w'q'}$, which in term would allow the use of equations 1.2 for $\bar{v}$, $\overline{\theta_v}$ and $\bar{q}$. However this is not directly possible because we don't have relations for computing some of the terms at the right side of equations 1.4, as the triple products in 1.4a or b. However, for certain types of flows there are semiempirical relations that associate these undetermined terms with variables that do have prognostic or diagnostic equations. This originate the turbulence models for the Reynolds equations, that can be classified in the following way:

Zero order models. In these cases, we suppose that prognostic variables are quasi stationary, and their respective prognostic equation reduce to diagnostic equations, that

can be integrated considering some hypothesis. In this way we can obtain explicit expressions for $\bar{u}$, $\bar{v}$, $\overline{\theta_v}$ and $\bar{q}$.

Zero order models are actually of great importance since they are reasonably realistic in the surface layer, and give relationships between the vertical profiles of $\bar{u}$, $\bar{v}$, $\overline{\theta_v}$ and $\bar{q}$ in the surface layer and the vertical turbulent fluxes in the surface layer and at the Earth's surface. This is the case for the Monin-Obukhov dimensionless relationships for the surface layer, which have an importance for the other PBL turbulence models that we shall explain bellow.

First order models. These models propose diagnostic relations for the vertical turbulent fluxes $\overline{w'u'}$, $\overline{w'v'}$, $\overline{w'\theta'}$ and $\overline{w'q'}$ of the Reynolds equations (1.2sed for forecasting $\bar{u}$, $\bar{v}$, $\overline{\theta_v}$ y $\bar{q}$. Usually, these models are based in the Boussinesq hypothesis, and propose diffusive equations for the turbulent fluxes,

$$\overline{w'\psi'} = K\frac{\partial \psi}{\partial z}$$

For the convective PBL case, there are convective eddies that have a vertical length scale of the order of the PBL height, so the dependency on a local vertical gradient proposed by this relationship had been criticized (Stull 1988). Nevertheless these models can be appropriate for cases where turbulence is generated mainly by wind shear, as is the case for the stable PBL.

Second and higher order models. In second order models $\overline{w'u'}$, $\overline{w'v'}$, $\overline{w'\theta'}$ y $\overline{w'q'}$ are prognosed with equations 1.4, which in turn requires semiempirical relationships for the undetermined terms that appear at their right hand sides. In third order models, equations 1.4 are also used for prognosing $\overline{w'u'}$, $\overline{w'v'}$, $\overline{w'\theta'}$ and $\overline{w'q'}$, but the undetermined terms

that appears in them are in turn prognosed with equations obtained through a procedure similar to the one used for deducing equations 1.4 These new equations also have undetermined terms that need for semi empirical diagnostic relations for the PBL case, as was the case for the models of first and second order.

Mixed layer models. This PBL models were pioneered by Lilly (1968), and are used in some AGCMs as is the case of the previous version of the UCLA AGCM PBL parameterization. This type of scheme compute bulk budgets of prognostic variables considering turbulent fluxes from Earth's surface, fluxes from PBL top due to mass entrainment of turbulence free air into the PBL, and horizontal large scale (non turbulent) fluxes within the PBL. PBL depth is also prognosed with a mass balance that consider PBL top mass entrainment and horizontal mass fluxes within the PBL.

Combined mixed-layer and higher order models. This type of models include the one described in this thesis. PBL depth is predicted in a similar way as in a mixed layer model, while several layers within the PBL allows for implementation of a first order, second order, etc. type of scheme .

Monin Obukov zero order relationships for the surface layer([2])

In the surface layer, the fact that vertical turbulent fluxes are considered constant in the vertical direction, combined with additional hypothesis proposed by Monin Obukov (1954), allow to find relationships in terms of dimensionless parameters (pi numbers) between the turbulent vertical fluxes and the vertical profiles of u, v, θ_v and q.

[2] Here after we assume that by default, any given variable ψ includes the time averaging.

Modifying arguments for boundary layers in incompressible fluids, the vertical shears of velocity and potential virtual temperature are related with other variables relevant to the turbulence process**. It is considered that** $\partial\vec{v}/\partial z$**,** $\partial\theta_v/\partial z$ **y** $\partial q/\partial z$ **are functions of:**

- **The height z respect to the Earth's surface,**
- **The vertical turbulent flux of horizontal velocity,**
- **The vertical turbulent flux of virtual potential temperature.**
- **The gravity acceleration g, which is relevant for the static stability, (as is the vertical flux of virtual potential temperature). We will consider its effects through the term** $\overline{w'\theta'_v}g/\theta_v$ **of the turbulent kinetic equation.**

(We assume for simplicity that there is only large scale horizontal velocity through the x direction.) The Buckinham theorem states that exist functions fu and fq of appropriate dimensionless variables, in particular such that

$$\frac{\partial u}{\partial z} = \frac{u_*}{z} f_u\left(\frac{z}{L}\right) \ , \ \frac{\partial q}{\partial z} = \frac{q_*}{z} f_q\left(\frac{z}{L}\right) \qquad (1.8)$$

were

$$u_* \equiv \left(\sqrt{(t_{turb})/r}\right)_{surf} \ , \ t_{turb} = \sqrt{r\left(\overline{w'v'}\right)^2 + r\left(\overline{w'u'}\right)^2} \ , \ q_* \equiv \overline{w'q'_v}/u_* \ , \ L \equiv \frac{\overline{w'q'_v}}{u_*^3 q_{v0}} g$$

There had been adjusted analytical expressions for the functions fu and fq using data form field experiments, and example of this is given by Bussinger et alt. (1971).

Integration of relations (2.25a,b) gives the vertical profiles u(z) y θ(z) as functions of $\overline{w'u'}$ $\overline{w'\theta'}$ and Earth's surface conditions. In particular it is supposed that at certain level zo u is zero (note that u in fact is a tlow frequency temporal average), this height depends

on the irregularities of the Earth's surface and is a measure of it roughness. It can be written in then

$$u(z) = u_* F_u\left(\frac{z}{z_o}, \frac{z}{L}\right),\ q\ (z) - q_o(z) = q_* F_q\left(\frac{z}{z_o}, \frac{z}{L}\right) \tag{1.9}$$

However, the problem of greater practical importance is in some sense inverse to this one: to find the vertical turbulent fluxes from the knowledge of u and q at some height z of the surface layer, and the surface conditions. Note that solving equations (2.25a,b) in u* y q* allows for this objective, and the resulting information is compiled in terms of the dimensionless variables u/u_*, $(\theta_v(z) - \theta_{v0})/\theta_*$, z/z_0 and the Richardson number Ri, defined as

$$Ri \equiv \frac{g\, z\left(q_v(z) - q_{v0}\right)}{u(z)^2 q_{v0}} \tag{1.10}$$

The results are expressed as the following aerodynamic formulas

$$\overline{w'u'}_0 = -C_u^2\left(\frac{z_o}{z}, \mathrm{Ri}\right)\left|\bar{u}(z)\right|\bar{u}(z) \tag{1.11a}$$

$$\overline{w'\theta'}_0 = C_\theta\left(\frac{z_o}{z}, -\mathrm{Ri}\right)C_u\left(\frac{z_o}{z}, -\mathrm{Ri}\right)\left|\bar{u}(z)\right|\left(\overline{\theta_v}(z) - \bar{\theta}_{v0}\right) \tag{1.11b}$$

and we can obtain analogously the following for the water vapor turbulent flux

$$\overline{w'q'}_0 = C_q\left(\frac{z_o}{z}, -\mathrm{Ri}\right)C_u\left(\frac{z_o}{z}, -\mathrm{Ri}\right)\left|\bar{u}(z)\right|\left(\overline{q}(z) - \bar{q}_0\right)\beta. \tag{1.11c}$$

There are also analytic expressions adjusted empirically for the functions Cu, C_θ y C_q, usually it is supposed that $C_\theta = Cq$. β is a coefficient of availability of moisture from the terrain. This coefficient is set to one for sea or wetland surfaces, and is close to zero in arid terrains. It should be noted that (1.11) assumes aerodynamic evaporation as the source of water from the Earth's surface, which is correct over sea. Over land,

transpiration from plants should be also accounted; this requires coupling the AGCM with a Land processes model. This goes beyond the scope of this work.

These formulas satisfy two important necessities for PBL prameterizations for atmospheric numerical models. First, they allow to establish the dependency of the vertical turbulent fluxes on the Earth's surface roughness. Direct simulation of these effects would be impractical for an atmosphere model. Second, models of order 2 and superior, as the mixed layer and combined models, require the prescription of these fluxes as boundary condition at the Earth's surface (see for example Mellor Yamada 1974). Even order 1 models fit the vertical fluxes in the rest of the PBL to the surface layer formulas for z-> 0 in order to account for the effects of roughness as given by zo.

Note that nevertheless the problem of computing the turbulent fluxes at Earth's surface is not yet closed, if we don't know the values of u, θ y q at some level z of the surface layer. This requires in turn of some model of the outer PBL as the ones mentioned above, in order to provide a boundary condition for the surface layer. An alternative procedure was proposed by Deardorff (1972). It consists in similitude relationship for the outer PBL similar to those considered for the surface layer, which take the value of the prognostic variables at a height z, supposed as the surface layer top, as boundary condition. Combining the relationship s for the surface layer with those of the outer PBL, the author obtains aerodynamic relationships for the turbulent fluxes at the Earth's surface analogous to (2.18a,b,c), but in terms of a bulk Richardson number for the whole PBL,

$$Ri_B \equiv \frac{g\,h\,(q_v - q_{v0})}{u^2\,q_{v0}} \qquad (1.12)$$

where h is the height of the whole PBL. The values of u and θ_v were considered at some level z of the surface layer now are representative values of the outer PBL.

Numerical studies of the PBL

Now we describe in a general way different numerical modeling approaches for the study of the PBL. These modeling studies (including those for the cloud topped PBL), fall mainly in three groups: higher-order closure models, large-eddy simulation (LES) models and mixed layer or "bulk" PBL models. Higher-order closure models involve the explicit prediction of turbulent kinetic energy (TKE), variances of the various quantities, and a number of covariances such as eddy fluxes (e.g. Moeng and Arakawa 1980; Bougeault 1985; Chen and Cotton 1987). In LES models, first used for a boundary layer simulation by Deardorff (1972), large turbulent eddies are explicitly resolved while smaller scale turbulence is parameterized (e.g. Deardorff 1980; Moeng 1986; Moeng et alt. 1996, Stevens et al. 1998). Lilly's (1968) pioneering bulk modeling of a cloud-topped mixed layer has been followed by many others (e.g. Schubert 1976; Schubert at alt. 1979; Randall 1980a, b; Stage and Businger 1981; Suarez et al. 1983; Nicholls 1984; Randall and Suarez 1984). In these models, a stratocumulus cloud deck occupies the upper portion of a well-mixed PBL and turbulence is primarily controlled by radiative cooling at the cloud top.

A review of the parameterization of the PBL processes in AGCMs

Many of the numerical studies of the PBL focus on the PBL itself, while the large-scale condition is more or less prescribed. The climate simulations on the other hand require two ways interactions between PBL scheme and the rest of the atmospheric simulated flow. PBL parameterization schemes used for these climate simulations are

based on either first or higher-order turbulence closures or on the mixed-layer formulation. The main objectives of PBL parameterization are computing the surface fluxes of the prognostic variables, determining if the PBL is cloud-topped or not, formulating the interactions between the PBL and the free atmosphere, and correspondingly determining the vertical structure of the PBL.

In the first-order closure schemes, a vertical profile of turbulent diffusivity is usually specified. Holstlag and Boville (1993) discuss the results of local and non-local schemes for vertical diffusion. In local schemes (e. g. Louis 1979; Louis et al. 1982), an eddy diffusivity coefficient is determined based on the vertical shears of velocity and static stability. The non-local schemes such as Troen and Mahrt (1986) and Hosltlag et al. (1990) utilize an eddy diffusivity profile of a given shape and an amplitude that depends on the bulk properties of the PBL. These schemes also incorporate the effects of transports by large eddies. The PBL height is diagnosed but mass entrainment through the PBL top is not explicitly computed.

In the first or higher-order closures schemes, the formulation of PBL clouds is usually based on an empirical diagnosis of relative humidity (Sundqvist 1978, Slingo 1982, Smith 1990) or a prognostic formulation of cloud liquid water (LeTruet and Li 1991, Del Genio 1996).

Lock et al. (2000) propose a PBL parameterization that has been implemented in climatic and mesoscale models. Each horizontal grid point is assigned to one of six PBL regimes by considering the buoyancy of undiluted parcels lifted from the Earth's surface or lowered from the top of the layer cloud closest to Earth's surface. PBL thickness and the existence and type of clouds within the PBL are also determined by these

considerations. Turbulent fluxes within the PBL are computed using a formulation of diffusivity coefficients that distinguish different PBL regimes considered. The parameterization includes a special formulation of the turbulent fluxes at PBL top that explicitly considers the entrainment rate parameterized following Lock (1998). Martin et al. (2000) discuss the results of testing this scheme in climate and mesoscale models. In particular, a developing version of the United Kingdom Meteorological Office (UKMO) Unified Model (UM) produced realistic stratocumulus cloud amounts, and improved boundary layer and cloud structures compared to earlier PBL parameterizations used at the UM. Mesoscale model simulations were also found to be improved in several aspects.

Mixed-layer models have also been implemented in AGCMs (Randall 1976; Suarez et al. 1983; Randall et al. 1989; Tokioka et al. 1984; see also Arakawa 2004). In these models, the PBL depth is explicitly predicted including computation of the mass entrainment through PBL top. The mass entrainment is also used for the computation of the fluxes of the prognostic variables into the PBL through its top. Among the most attractive aspects of these schemes is that the interactions between the PBL and the free atmosphere can be explicitly formulated, and so are the processes associated with stratocumulus inside the PBL. Stratocumulus cloud decks occur above the lifting condensation level when this is within the PBL, and radiative cooling at the cloud top controls the turbulence and the mass entrainment from the free atmosphere.

Stevens (2002) examines the entrainment processes for a stratocumulus cloud-topped PBL. He discusses several entrainment formulas, and the way in which these include the TKE generation, the TKE fraction that is used to overcome the stratification capping the cloud-topped PBL, and take into account other non-turbulent processes. The discussion

includes the formulations by Lock (1998), Turton and Nicholls (1987), Moeng (2000), Lilly (2002) and Randall and Schubert (2004). The entrainment formulation proposed by Randall and Schubert (2004) is a part of the PBL parameterization used in this work.

The breakup of a stratocumulus deck can be due to several processes. Those involved in the transition from the marine stratocumulus regimes observed over the eastern oceans to the trade cumulus regimes are of great importance in view of the low-level cloudiness. Randall (1976, 1980a, b) and Deardorff (1980) proposed the cloud-top entrainment instability (CTEI) as a possible mechanism for the destruction of a uniform cloud layer. When the evaporative cooling at the cloud top overcomes the stability associated with the inversion above, the entrained air has negative buoyancy at the inversion base, and consequently additional TKE is generated promoting further entrainment. It is proposed that this condition leads to a runaway destruction of the cloud due to the rapid infusion of dry air. However, this mechanism does not include the effect of partial cloud cover, which limits its possibility of describing the breakup of a uniform cloud layer (Randall and Schubert 2004). Krueger et al. (1995) discusses a simulation of the Lagrangian evolution of the boundary layer under conditions typical of July over the Pacific Ocean southwest of California, using the University of Utah Cumulus Ensemble Model. This simulation involves the translation of the domain along the climatological boundary layer trajectory at a rate equal to the observed wind speed, with prescribed changes in SST and large-scale forcing. The results show a transition from overcast to broken and finally scattered clouds; cloud cover decreases from 100% at the start to about 20% at the end of six days. A layer of cumulus clouds under the stratocumulus layer is present after two days. This appears to correspond to the intermediate stage in the stratocumulus transition

(Bretherton 1992). It was also found that changes in the structure of the simulated PBL with the formation of two decoupled layers start before the transition of the cloud patterns. Also the role of buoyancy forces in driving the PBL turbulence changes; the negative buoyancy associated with downdrafts becomes less important, while the positive buoyancy in updrafts becomes more important. This is not consistent with the role of CTEI mechanism in the transition from the marine stratocumulus to shallow and trade cumulus regimes.

The main limitation of the mixed-layer approach is that it doesn't consider wind shears and deviations of the potential temperature and water-mixing ratio from vertically homogeneous profiles. Acknowledging this point may facilitate simulations of PBL regimes with secondary internal inversion (decoupled regimes) and shallow cumulus effects.

In the framework traditionally used in the UCLA AGCM, the lowest model layer is assigned to the PBL (Suarez *et al.* 1983). The depth of this layer is predicted through the mass budget equation including the PBL-top entrainment, cumulus mass flux and horizontal mass convergence within the PBL. When the entrainment and cumulus mass flux become zero, the PBL-top becomes a material surface, keeping the PBL air separated from the free atmosphere air. The UCLA AGCM using this framework has been applied to many climate studies, particularly in research on air-sea interactions for which the AGCM was successfully coupled to ocean GCMs (Mechoso *et al.* 2000). Motivated by this success, Konor and Arakawa (2005) introduced a new framework, which maintains the advantages of the mixed-layer formulation while relaxing the mixed-layer constraint by introducing several layers within the PBL. Figure 1 is a schematic depiction of this

framework. Explicit prediction of vertical shear within the PBL is expected to have a major impact on the evolution of extratropical baroclinic disturbances. It also has a potential for capturing the rich variety of cloud types in the tropics, such as those described by TRMM data and the data gathered during an EPIC 2001 cruise (Bretherton et al. 2004).

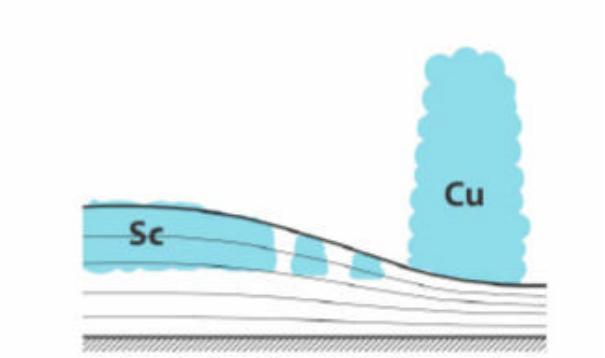

FIG. 1. A Schematic depiction of the vertical structure of the PBL with the new scheme.

The PBL scheme of Konor and Arakawa (2005 and 2008) has aspects in common with the one proposed by Grenier and Bretherton (2001). The latter scheme also predicts the height of the inversion layer that caps a convective PBL using the mass budget equation, as in the mixed layer formulation. The internal vertical structure of the PBL is then obtained by using turbulent fluxes computed with a 1.5-order closure based on Mellor and Yamada (1982). Tests of the scheme using a single column model with both coarse and fine vertical resolutions showed that it could successfully simulate the dry-convective PBL with both resolutions. However, simulation of the cloud-topped PBL was found satisfactory only for resolutions of 15 hPa or less. A major difference between Konor-Arakawa and Grenier-Bretherton schemes is that the PBL top in the former shares a

coordinate surface with the free atmosphere, while in the latter the PBL top floats between model's coordinate surfaces.

In the new framework being presented here, PBL processes are parameterized following a new approach. The effects of large convective eddies are represented by a bulk formulation, which includes prediction of TKE, and the effects of small eddies that are mostly diffusive are represented by a K-closure formulation that uses a diffusivity coefficient profile based on Holtslag and Boville (1993). The PBL-top mass entrainment is explicitly computed with a formulation proposed by Randall and Schubert (2004). The surface fluxes of momentum, heat and water vapor are determined by an aerodynamic formula, in which both the square root of TKE and the mean large-scale PBL velocity are used to determine the velocity scale. With this formulation, the surface fluxes estimates are expected to be better than the traditional methods because the grid-scale wind can be weak while the convective mixing is strong.

The new PBL parameterization scheme is tested with the uncoupled and coupled climate simulations. The present paper illustrates the behavior of the PBL in an actual climate simulation with the uncoupled UCLA AGCM. While the comparison between simulation and observation can tell us a great deal about the overall quality of the PBL parameterization scheme, it alone cannot confirm the impact of individual processes or interactions. We therefore show results from two additional experiments. In the first experiment, the effects of radiative cooling at the PBL top (in the presence of PBL clouds) on TKE generation and entrainment rate are turned off. This experiment is extended by additionally eliminating the effect of radiative cooling on the potential temperature of the uppermost PBL layer. In the second experiment, the model's vertical

structure is changed to the conventional sigma coordinate, i.e. the definition of sigma levels are independent of the PBL top. In this case, the PBL depth and turbulent fluxes are determined through the diagnostic equation given by Troen and Mahrt (1986) and the non-local flux formulation proposed by Holtslag and Boville (1993), respectively.

The PBL parameterization we are presenting in this paper does not fully benefit from the potential of the multi-layer framework. We believe that the benefit of the multi-layer framework is not fully realized before we predict TKE for each layer and incorporate a scheme to represent cumulus roots. At this stage, what we can realistically expect from the multi-layer framework is an improvement in the simulated vertical wind shear within the PBL and, as a consequence, the effect of low-level baroclinicity.

The text of this thesis is organized as follows: sections 2 and 3 describe the PBL parameterization and its implementation in the UCLA AGCM. Section 4 shows the results of a multiyear simulation with the model. Section 4 presents the cloud-radiation/turbulence/thermodynamics interactions with the new PBL parameterization, and discusses the results of experiments that demonstrate the importance of those interactions. Comparisons of the results obtained using new and previous parameterizations are also presented in section 4. Section 5 compares the results obtained by a first-order turbulence closure scheme with diagnostic determination of clouds and our new PBL parameterization scheme. Section 6 gives a summary and discussion of the results, and a preview of developments.

2. The Proposed Parameterization of PBL processes

A basic aspect of the PBL parameterization described in this thesis, is that vertical extent of the PBL, PBL height, is predicted from a mass balance that considers both horizontal convergence of mass within the PBL and mass entrainment into the PBL through its top from the turbulence free atmosphere above it. We define E as this mass entrainment rate, its units are mass over surface and time. We note p_B as the pressure at PBL top, p_S as the pressure at earth's surface, and $\pi_{PBL}=p_S-p_B$,. If we accept hydrostatic balance, then π_{PBL} is the PBL mass per unit of area multiplied by g, gravity acceleration (on a given point of the horizontal domain and on a given instant). The vertically integrated mass balance equation that allows for the prediction of PBL thickness (in terms of pressure thickness) can be written as

$$\frac{\partial p_{PBL}}{\partial t} + \frac{1}{p_{PBL}} \int_{p_B}^{p_S} \nabla.(p_{PBL}\vec{v})dp + gE = 0 \qquad (2.1)$$

where v is the horizontal component of the velocity field.

From this equation it becomes clear that entrainment rate is a key variable of the parameterization. The described approach is common with the mixed layer type of parameterization. As an improvement to mixed layer approach, this scheme allows for multiple layers within PBL height, which gives a framework that enables explicit discussion of mixing processes and also departures from completely well mixed profiles assumed in the mixed layer approach.

Entrainment at PBL top as other important quantities necessary to close our parameterization, are considered to depend on vertical average of TKE through the PBL, which we define as

$$e_{PBL} \equiv \frac{g}{p_{PBL}} \int_{z_S}^{z_B} r e dz \qquad (2.2)$$

(here z_S and z_B are heights of Earth's surface and PBL top respectively). The prediction equation for e_{PBL} can be deduced from equation (1.1) for non vertically averaged TKE. This is shown in Appendix A. The resulting equation is

$$\frac{\partial e_{PBL}}{\partial t} = \frac{g}{p_{PBL}} \left[k \int_{p_B}^{p_S} \frac{r \overline{w's_v'}}{p} dp + \int_{z_S}^{z_B} \left(r \overline{w'u'} \frac{\partial u}{\partial z} + r \overline{w'v'} \frac{\partial v}{\partial z} \right) dz - \int_{z_S}^{z_B} r e \, dz \right] + \frac{e_{PBL}}{p_{PBL}} \int_{p_B}^{p_S} \frac{\nabla . (p_{PBL} \vec{v})}{p_{PBL}} dp - \frac{gE}{p_{PBL}} = 0 \qquad (2.3)$$

Term $\frac{g}{p_{PBL}} \int_{p_B}^{p_B} \frac{r \overline{w's_v'}}{p} dp$ is the *buoyancy generation term*,

term $\frac{g}{p_{PBL}} \int_{Z_S}^{Z_B} \left(r \overline{w'u'} \frac{\partial u}{\partial z} + r \overline{w'v'} \frac{\partial v}{\partial z} \right) dz$ is the *shear generation term*,

term $\frac{g}{p_{PBL}} \int_{p_B}^{p_B} r e dz$ is the *dissipation term*,

term $\frac{e_{PBL}}{p_{PBL}} \int_{p_B}^{p_B} \frac{\nabla . (p_{PBL} \vec{v})}{p_{PBL}} dp$ is the horizontal convergence of ePBL and $-\frac{gE}{p_{PBL}}$ is the effect of income of air free of turbulence trough mass entrainment at PBL top. This term is set to zero in case of E<0.

For applying equation 1.4 we need formulas for buoyancy, shear and dissipation terms, besides a formulation for E. We next focus on the basis for such formulas.

(2.1) Turbulent fluxes of thermodynamics quantities (q, q, s, s_v)

We consider that (vertical) turbulent fluxes are due to two different processes: convective eddies, that occur when PBL is convectively unstable, and small scale eddies, which arise from shear of the large scale flux or the convective eddies when they exist. Convective

eddies can be as large as the vertical extent of the PBL, and we also call them large scale eddies in the present discussion. They affect mostly thermodynamic variables, q, q or r=q+l and h. Small scale eddies are always present if at least some turbulence exists, and affect both thermodynamic variables and horizontal velocity, v.

(2.1a) Turbulent fluxes due to large scale eddies

The considerations that follow strictly apply for convective unstable PBLs. A basic hypothesis of convectively unstable PBL is that, in absence of condensation, either virtual potential temperature or virtual dry static energy, and water vapor mixing ratio, q, are nearly well mixed within the PBL, that is

$$\frac{\partial q_v}{\partial z} = 0 \;\; or \;\; \frac{\partial s_v}{\partial z} = 0 \;\; and \;\; \frac{\partial q}{\partial z} = 0$$

If condensation actually occurs within the PBL, a stratocumulus cloud deck will develop between lifting condensation level and PBL top. In such cases, neutral profiles are expressed in terms of h_v and r, total water mixing ratio. r = q + l, l is the liquid water mixing ratio.

$$\frac{\partial h_v}{\partial z} = 0 \;\; and \;\; \frac{\partial r}{\partial z} = 0 \qquad (2.4)$$

Note than in absence of condensation, r = q, so vertical well mixing of r is the same as vertical well mixing of q. Besides this, since sv = hv $-$Lq, well mixing of hv and r leads also to well mixing of sv. Then, the neutral conditions given above for the condensation case includes the ones for no condensation as a particular case.

The well mixed hypothesis in turn gives foundation for a hypothesis about vertical turbulent fluxes of these variables. We assume that vertical convergence is the main source of tendency for these variables. Then, if

$$\frac{\partial h_v}{\partial t} = -\frac{\partial\left(\overline{w'h_v'}\right)}{\partial z} + [other\ \ terms] \quad and \quad \frac{\partial r}{\partial t} = -\frac{\partial\left(\overline{w'r'}\right)}{\partial z} + [other\ \ terms]$$

and firsts terms in the right side of these equations prevail over the others, since conservation of a well mixed profile of hv and r require a well mixed profile also of its tendencies, vertical convergence of turbulent fluxes have to be well mixed as well.

$$\frac{\partial\left(\overline{w'h_v'}\right)}{\partial z}\ const.\ with\ height,\ and\ \frac{\partial\left(\overline{w'r'}\right)}{\partial z}\ const.\ with\ height$$

Therefore, vertical turbulent fluxes themselves must have vertical profiles which are linear with height. Knowledge of these turbulent fluxes at PBL top and at Earth's surface allows for computing them at any level of the PBL from linear interpolation. If we consider p as a vertical coordinate, turbulent fluxes of h_v and r can be computed at any level p as:

$$\overline{w'h_v'} = \frac{p_s - p}{p_s - p_B}\left(\overline{w'h_v'}\right)_B + \frac{p - p_B}{p_s - p_B}\left(\overline{w'h_v'}\right)_S \qquad (2.5a)$$

$$\overline{w'r'} = \frac{p_s - p}{p_s - p_B}\left(\overline{w'r'}\right)_B + \frac{p - p_B}{p_s - p_B}\left(\overline{w'r'}\right)_S \qquad (2.5b)$$

Linear interpolation of h and r fluxes obtained at PBL top (as it will be discussed in section 2.2) and from from Earth's surface (according to Monin Obukov type of surface layer relations hips, to be discussed in section 2.3) give turbulent flux of h and r in the whole vertical domain of the PBL. From them, we deduce fluxes of s and q as we will see next. These fluxes in turn allows for computing flux of s_v, necessary for closing turbulent kinetic energy equation.

In case of cloud free PBL, r=q, and since in any case s = h – Lq, we have

$$\overline{w'q'} = \overline{w'r'} \tag{2.6a}$$

$$\overline{w's'} = \overline{w'h'} - L\overline{w'q'} \tag{2.6b}$$

From definition of virtual potential temperature we can deduce the turbulent flux of virtual static energy from those of s and g, resulting in

$$\overline{w's_v'} = \overline{w's'} - 0.608T\,\overline{w'q'} \tag{2.7}$$

If PBL is cloud topped, (2.6a,b) and (2.7) apply below the condensation level. Above condensation level, we assume that parcels that came either from bellow or above are saturated, as well as their environment, and then q equals saturation water vapor mixing ratio at the temperature and pressure conditions of any parcel. Lets T' be the difference of any given parcel temperature from the environment temperature. Since parcel and environment are at equal pressure, and we assume T' small enough, we have that perturbation of q is

$$q' = q_*' = \left(\frac{\partial q_*}{\partial T}\right)_p T'$$

If we define

$$g \equiv \frac{L}{c_p}\left(\frac{\partial q_*}{\partial T}\right)_p, \tag{2.8}$$

$$\overline{w'q'} = \frac{g c_p}{L}\overline{w'T'} = \frac{g}{L}\overline{w's'} \;\therefore\; \overline{w's'} = \overline{w'h'} - L\overline{w'q'} = \overline{w'h'} - g\,\overline{w's'} = \overline{w's'}$$

and then

$$\overline{w's'} = \frac{1}{1+g}\overline{w'h'} \tag{2.9a}$$

$$\overline{w'q'} = \frac{g}{L(1+g)}\overline{w'h'} \tag{2.9b}$$

Therefore turbulent fluxes of both s and q are now "anchored" to the turbulent flux of h. As seen, the interpretation of this lays in the fact that when condensation occurs, q=q*, and q*' is controlled by T' as shown, so q'* becomes controlled by h' through the γ parameter. (In fact in a well mixed PBL, h controls evolution of T with height, and q* itself is mostly controlled by T since it depends strongly on T and relatively weakly on p, within the variations that T and p have within the PBL.) Turbulent flux of virtual static energy can be computed as

$$\overline{w's_v'} = b\,\overline{w'h'} - c_p T\,\overline{w'r'} \quad with \quad b \equiv \frac{1+1.608\,c_p T g\,/L}{1+g} \tag{2.10}$$

(2.1b) Turbulent fluxes due to small scale eddies

Small scale eddies affect the prognostic equations of v, q and r. We evaluate them from a diffusive, K type of relation,

$$?\left(\overline{w'?'}\right)_{small\ scale} = -?K\,\frac{\partial ?}{\partial z}\,.$$

For the computation of the diffusion coefficient, we use a scheme based in Troen and Martin (1986). Within a convective mixed layer, small eddies are generated primarily through energy cascade from larger eddies and, therefore, their properties depend on bulk parameters such as the PBL height or some turbulent velocities scale computed from Earth surface fluxes. Close to the ground, velocity shear is important for generating turbulence. Considering these, Troen and Martin propose diffusivity coefficients for momentum and thermodynamics variables that depend on whether the PBL is convectively unstable or stable with respect to the earth surface temperature. For both cases, they propose formulas of the diffusivity for the PBL region close to Earth's surface, and for the region away from Earth's surface. Our formulation of K changes the

choice4 of these authors for the turbulent velocity scale, using instead the square root of TKE. In the Appendix B we show our K formulation.

(2.2) Turbulent fluxes at PBL top

For convectively unstable PBLs, strong discontinuities of prognostic variables occur at the top. In particular potential temperature increases in a span of few meters above PBL, (while water content decreases sharply). This strong increase of potential temperature with height (thermal inversion) makes this thin layer at PBL top very stable in static terms, and this defines a clearly defined limit for turbulence region in the vertical direction.

The case of stratocumulus cloud toped PBL requires the acknowledgement of an additional fact. Stratocumulus cloud effectively radiates in the long wave range upwards from its upper bound, at PBL top, and downwards from cloud base. Downward long wave radiative flux is nearly compensated by upward radiation from Earth's surface, while in case of clear sky above stratocumulus upward radiation is not compensated, but goes mostly to outer space. This results in a strong cooling concentrated also at PBL top, which can amount to 100 watts/m2. Such cooling has a fundamental consequence, it generates convective instability through the PBL since it occurs above, facilitating entrainment, driving convective eddies and thus generating turbulent kinetic energy. The two former effects are represented through a concentrated sink of sensible heat at PBL top that contribute to positive vertical turbulent fluxes of buoyancy, as we see next.

Let ψ be any mass specific prognostic variable like h_v, s_v, r or q. Then transport of y at PBL top is due to entrainment and vertical turbulent fluxes. We assume that the thin layer were discontinuities take place is thin enough to neglect accumulation of mass or

mass weighted properties. We call B+ the top of the thin transition layer, right above PBL top (B level), and B- its bottom, right below B. In absence of sources of ψ within this layer, we can consider an income of mass weighted ψ, $E\psi_{B+}$, form above, and output $E\psi_{B-}$, and an income due to vertical turbulent flux at B-, $\left(r\overline{w's'}\right)_{B-}$ We don't account for vertical turbulent fluxes at the level B+, since this is already in the turbulent free region above the PBL. Then in absence of concentrated sources or sinks for y at the transition layer, the neglect of accumulation leads to $Ey_{B+} - Ey_{B-} + \left(r\overline{w'y'}\right)_{B-} = 0$, and hence

$$\left(r\overline{w'y'}\right)_{B-} = -E\left(y_{B+} - y_{B-}\right) \tag{2.11a}$$

This formula allows for computation of turbulent fluxes at PBL top, and therefore is of crucial importance for the parameterization closure. Absence of concentrated sources is always correct for q, r, and is also correct for s and h in case of cloud free PBL. In case of stratocumulus topped PBL, let ΔR (defined positive) be the net radiative cooling per unit of time and area at PBL top. This is a concentrated source for turbulent flux of s and h, and so

$$\begin{aligned} &Es_{B+} - Es_{B-} + \left(r\overline{w's'}\right)_{B-} - \Delta R = 0 \;\therefore\; \left(r\overline{w's'}\right)_{B-} = -E\left(s_{B+} - s_{B-}\right) + \Delta R \\ &Eh_{B+} - Eh_{B-} + \left(r\overline{w'h'}\right)_{B-} - \Delta R = 0 \;\therefore\; \left(r\overline{w'h'}\right)_{B-} = -E\left(h_{B+} - h_{B-}\right) + \Delta R \end{aligned} \tag{2.11a,b}$$

Note that radiation cooling ΔR positively contributes to vertical buoyancy flux. Its contribution for balance of s or h is certainly negative, but since cooling from above produces negative perturbations of s of q (s'<0, q'<0), and this cooled particles tend to sink, (w'<0) w's' or w'q' are positive, in such way that cooling from PBL top has, qualitatively, the same effect on convective turbulence generation than a warming from bellow as expressed.

2.3 Formulation of the Earth's surface fluxes

The surface fluxes of momentum, temperature and moisture are determined from an aerodynamic formula, which is modified version of that proposed by Deardorff (1972). Our formulation considers both the square root of the bulk TKE and the mean large-scale PBL velocity to determine the velocity scale. With this formulation, the surface fluxes are expected to be better estimated compared to the traditional methods, since the mean wind can be weak while the convective mixing is strong. The fluxes of momentum, temperature and moisture are computed as follows:

$$\left.\begin{aligned} F_v &= \rho_s C_U C_U \max\left(u_M\,,\ \alpha_1\sqrt{e_{PBL}}\right) v_M \\ F_\theta &= \rho_s C_U C_T \max\left(u_M\,,\ \alpha_2\sqrt{e_{PBL}}\right)(\theta_G - \theta_M) \\ F_q &= \rho_s C_U C_T \max\left(u_M\,,\ \alpha_2\sqrt{e_{PBL}}\right)(q_G - q_M)\,k \end{aligned}\right\}. \qquad (2.12a,b,c)$$

where C_U and C_T are coefficients that depend on the bulk Richardson number, the PBL thickness and the surface roughness length, as in Deardorff (1972), θ_G is the potential temperature at the Earth surface and q_G is the saturation moisture at the Earth's surface temperature and pressure. k is a coefficient of water availability of the terrain. This coefficient is one in water surfaces, and close to zero in arid terrains. u_M is the module of the lower-most layer velocity. We are currently using $\alpha_1 = 12.5$, and $\alpha_3 = 9.5$. We assume that next to Earth's surface there is not saturation (this will be discussed further in next section), so turbulent flux of q is equivalent to turbulent flux of r. Turbulent flux of s is computed from that of θ. These fluxes allow the computation of turbulent flux of h through equation 2.6b.

(2.4) Entrainment formulation

The entrainment formulas used in our parameterization are proposed by Randal and Schubert (2004). The formulas recognize whether the PBL is cloud-topped or not, and whether TKE is above the allowed minimum TKE_{min} or below. Here we give the formulas considered and in the Appendix C we give a detailed deduction of the formulas.

If TKE is above the TKE_{min} value, which is taken as $0.01 m^2/s^2$, we consider that there is a positive turbulent mass entrainment E. If the PBL is cloud free, it is computed as

$$E = b_1 \frac{r\Pi_B q_{PBL} e_{PBL} \sqrt{e_{PBL} - e_{\min}}}{\Pi_B q_{PBL} e_{PBL} + g(dz)_{PBL}(s_{vB+} - s_{vB-})} \qquad (2.13a)$$

where b1 is a parameter taken as 0.4, Π_B is the Exner function at the B level (defined as $\Pi \equiv c_p (p/p_o)^{R/c_p}$.), $(\delta z)_{PBL}$, ρ_{PBL} and θ_{PBL} are PBL thickness (in terms of length), and the density and the potential temperature vertically averaged over the PBL. $s_{v\,B-}$ and s_{vB+} are the virtual static stability computed B_+ and B- levels.

In the case of a cloud-topped PBL, entrainment formula accounts for the effect of both radiative cooling at PBL top and evaporative cooling of the entrained parcel. Since entrained parcel comes from free atmosphere above the PBL, they are drier than PBL air, and when they enter into PBL stratocumulus cloud, evaporation of cloud water droplets into this relative dry parcels occurs, demanding latent heat, hence the evaporative cooling. Evaporative cooling per unit of entrained mass can be computed as

$$(\Delta s_v)_{crit} = \frac{(L - 1.608\Pi_B \theta_{B+})(q^*(T_{B+}, p_B) - q_{B+})}{(1 + \gamma_{B+})}$$

It is assumed that effective Δs_v for entrainment computation should had this quantity substracted. In a similar way, entrained particle undergoes a cooling that can be assessed as

$\Delta T_{rad} = \Delta R / \left(c_p E \right)$, from which it can be concluded

$$c_p \Delta T_{vrad} = \Delta s_{vrad} = b_B \Delta R / E$$

And from this we obtain a formula that allows for computing entrainment for stratocumulus topped PBL in analogous way as the cloud free case, but substracting to static stability the effects of radiative and evaporative cooling, obtaining a kind of "effective" static stability:

$$E = b_1 \frac{r \Pi_B q_{PBL} e_{PBL} \sqrt{e_{PBL} - e_{\min}}}{\Pi_B q_{PBL} e_{PBL} + g(dz)_{PBL} \left[\left(s_{vB+} - s_{vB-} \right) - \Delta s_{vcrit} - b_B \Delta R / E \right]}$$

This expression has E in both sides, with simple operations from it we obtain

$$E = \frac{b_1 r \Pi_B q_{PBL} e_{PBL} \sqrt{e_{PBL} - e_{\min}} + b_B g(dz)_{PBL} \Delta R}{\Pi_B q_{PBL} e_{PBL} + g(dz)_{PBL} \left[\left(s_{vB+} - s_{vB-} \right) - \Delta s_{vcrit} \right]} \qquad (2.13b)$$

where ? $_{PBL}$ and ? $_{PBL}$ are vertically averaged in the sub-cloud layer, b_1 is taken as 0.4.

When the prognostic equation for TKE forecasts a value lesser than TKE_{min}, TKE_{min} is taken instead, and the PBL is considered to detrain mass at a constant rate that corresponds to 250 hPa in 3 hours.

(2.5) Closure terms for e_{PBL} equation

We next focus on the necessary terms for closing e_{PBL} equation, vertical average of the s_v turbulent flux discussed above, and the shear and dissipation terms.

We define $B \equiv k \int_{p_B}^{p_S} \frac{r\overline{w's'_v}}{p} dp$, the buoyancy term of equation (2.3). For the cloud free PBL, considering that turbulent flux of sv varies linearly through the PBL, B is computed as

$$B = k \frac{(p_S - p_B)\left(\overline{w's'_{vS}} + \overline{w's'_{vB}}\right)}{p_S + p_B} \qquad (2.14a)$$

where we have approximated the pressure in the integrand by its vertical mean value over the PBL. For the cloud-topped PBL,

$$B = k \frac{(p_C - p_B)\left(\overline{w's'_{vC+}} + \overline{w's'_{vB}}\right)}{p_C + p_B} + k \frac{(p_S - p_C)\left(\overline{w's'_{vS}} + \overline{w's'_{vC-}}\right)}{p_S + p_C} \qquad (2.14b)$$

where sub indexes C+ and C- indicate that flux of virtual dry static energy are computed immediately above and bellow the condensation level (p_C). Since C+ and B levels are above condensation level, and S and C- levels are below, the respective functions discussed above are used. This results on a discontinuity of the flux at C level. Note also that in the case of a cloud-topped PBL, computation of turbulent flux of s_v includes the radiative cooling effects at the PBL top. When the PBL is not cloud topped, the main driving of the TKE buoyancy generation is the flux from the surface.

The shear production of TKE $S \equiv \int_{z_s}^{z_B} \left(r\overline{w'u'}\frac{\partial u}{\partial z} + r\overline{w'v'}\frac{\partial v}{\partial z} \right) dz$ is computed as

$$S = \alpha\left(\rho_S |Fv|_S \cdot \mathbf{v}_S + \frac{1}{2} E\left(\mathbf{v}_{B+} - \mathbf{v}_{B-}\right)^2 \right), \qquad (2.15)$$

where Fv is the flux of momentum at the earth surface, $\mathbf{v}_{B+}$ and $\mathbf{v}_{B?}$ are the velocities immediately above and bellow the PBL top, respectively. α is a coefficient that tends to zero when the PBL thickness grows Here we assume that TKE generated near the Earth's

surface is locally dissipated so that shear contribution to TKE is relevant only when the PBL is thin. The dissipation term is computed from

$$D = C\rho_{PBL}\left(e_{PBL}\right)^{3/2}, \qquad (2.16)$$

where the coefficient C is taken as 1.0.

Additional comments on closure

As could be seen, TKE requires computation of entrainment rate (for the fluxes at PBL top and also for earth's surface fluxes), and reciprocally entrainment formulation requires TKE prediction. Model integration assumes that entrainment diagnose can be carried on with TKE of the immediately previous time step, and then used for the actual time step prediction. The strong interaction between TKE and entrainment result into a stabilizing feedback. For the cloud free case, positive entrainment is associated with negative fluxes of buoyancy at PBL top. Larger values of TKE correspond to larger values of entrainment, but this in turn provokes negative buoyancy that destroys TKE. This mechanism controls grow of both TKE and entrainment rate. Besides this, it is observed that the grater PBL thickness grows, the greater Δs_v tends to be, increasing negative buoyancy associated with any given positive entrainment rate. Then PBL will grow until either horizontal mass divergence compensates entrainment rate, or until viscous dissipation and negative buoyancy at PBL top, combined, led TKE to small values, preventing further entrainment.

Stratocumulus cloud topped PBL is also more affected by radiative contribution to buoyancy flux, as discussed above. Despite negative contribution associated with entrainment of warmer parcels (given by $-E\Delta s_v$), evaporative cooling and radiative cooling usually lead to positive buoyancy fluxes at PBL top. Note that this is less so for

taller PBL tops, since Δs_v tends to increase with PBL top height. Marine stratocumulus clouds tend to occur at regions of relatively high low level mass divergence, and PBL tends to grow until entrainment compensate horizontal mass divergence that occurs through the entire PBL height.

3 General description of the UCLA AGCM with the new PBL parameterization.

The UCLA AGCM is a finite difference model that integrates the primitive equations of the atmosphere. The model's horizontal discretization is based on the Arakawa C grid, and the vertical discretization follows Arakawa and Suarez (1983). The parameterization of physical processes other than those of the PBL will be referred in the next section. We describe next the equations for the prognostic variables, with emphasis on their discretization within the PBL. Discretization of prognostic equations for the free atmosphere is discussed in the BID-CONICYT 117 report.

3.1 Continuous governing equations

We start by the definition of the s vertical coordinate. We define p_B as the pressure at the top of the PBL. Thus the region between p_S and p_B, where p_S is the pressure at the Earth surface, represents the PBL. In the free atmosphere above the PBL, we consider two regions. One between the PBL top and a tropopause level at $p = p_I$, and the other between p_I and the model top, at $p=p_T$. The definitions of the σ coordinate in these three regions are:

$$s \equiv 1+\frac{(p-p_B)}{(p_S-p_B)} \quad for \quad p_B \le p \le p_S \tag{3.1a}$$

$$s \equiv \frac{(p-p_B)}{(p_B-p_I)} \quad for \quad p_I \le p \le p_B \tag{3.1b}$$

$$s \equiv \frac{(p-p_I)}{(p_I-p_T)} \quad for \quad p_T \le p \le p_I \tag{3.1c}$$

We currently use p_T = 1 hPa and p_I = 100 hPa. According to these definitions, σ = -1

at the model top ($p = p_T$), $\sigma = 0$ at the tropopause level ($p = p_I$), $\sigma = 1$ for the PBL top ($p = p_B$), and $\sigma = 2$ at the earth surface ($p = p_S$). Note PBL top results then a coordinate surface. This arrangement facilitates simulation of processes concentrated near the PBL top, such as mass entrainment and radiative cooling, since it becomes more straightforward to obtain discontinuities of several variables at this level which are of crucial importance, as was found above. More traditional definitions of sigma coordinate also allow for this type of computations, although in such cases special additional considerations would be necessary for the implementation of a scheme as the one described here (see for instance Bretherton at al. 2001)

From the definitions of sigma coordinate given here the pressure can be obtained as

$$p = p_S - (\sigma_S - \sigma)\pi_{PBL} \quad \text{for} \quad \sigma_S \geq \sigma \geq \sigma_B \ , \ \text{with} \ \pi_{PBL} = p_S - p_B \qquad (3.2a)$$

$$p = p_I + \sigma\pi_{trop} \quad \text{for} \quad \sigma_B \geq \sigma \geq \sigma_I , \ \text{with} \ \pi_{trop} = p_B - p_I \qquad (3.2b)$$

$$p = p_I + \sigma\pi_{strat} \quad \text{for} \quad \sigma_I \geq \sigma \geq \sigma_T , \ \text{with} \ \pi_{strat} = p_I - p_T \qquad (3.2c)$$

Note that since we accepted hydrostatic approximation, in any given point of the horizontal domain and time π_{PBL} is the mass per unit of horizontal area of the PBL, multiplied per g, while $\pi_{PBL}+\pi_{trop}+\pi_{strat}$ is the mass per unit of area, multiplied by g, of the whole atmosphere. The mass continuity equation can be written as

$$\frac{\partial p}{\partial t} + \nabla.(p\,\vec{v}) + \frac{\partial(p\dot{s})}{\partial s} = 0 \qquad (3.3)$$

where π is either π_{PBL}, π_{trop} or π_{strat}

The thermodynamic equation in terms of the potential temperature ? is, within the PBL,

$$\frac{\partial(p_{PBL}q)}{\partial t}+\nabla.(p_{PBL}q\,\vec{v})=-\frac{\partial(p_{PBL}q\dot{s})}{\partial s}+\frac{p_{PBL}Q}{\Pi}+G_q \qquad (3.4a)$$

where G_θ is the contribution of the turbulent fluxes to the tendency of θ, to be discussed next, and Q is the heating rate. In the free atmosphere,

$$\frac{\partial(pq)}{\partial t}+\nabla.(pq\,\vec{v})=-\frac{\partial(pq\dot{s})}{\partial s}+\frac{pQ}{\Pi} \qquad (3.4b)$$

where π is π_{trop} or π_{strat} according to the respective free atmosphere regions.

The continuity equation for the total water inside the PBL predicts the water mixing ratio (r), which is the water vapor mixing ratio (q) plus the liquid water mixing ratio (l). Here we assume that PBL turbulence allows the air to hold both phases of water. This assumption is escencially correct for cloud droplets up to certain sizes, when droplets exceed certain sizes, actually light precipitation occurs in form of drizzles. Drizzles are not considered in current scheme, and no large-scale precipitation processes occur within the PBL unless the pressure at the condensation level is greater than the surface pressure (condensation level bellow the earth surface). If this occurs, large-scale precipitation is computed to make the condensation level equal to the surface level. The continuity equation for r within the PBL is

$$\frac{\partial(p_{PBL}r)}{\partial t}+\nabla.(p_{PBL}r\,\vec{v})=-\frac{\partial(p_{PBL}r\dot{s})}{\partial s}-p_{PBL}C_r+G_r \qquad (3.5a)$$

where G_r is the contribution of the vertical convergence of the turbulent flux of r, and C is the precipitaion rate per unit of time and mass, with the limitations expressed above. For the free atmosphere, water mixing ratio continuity equation is expressed in terms of water vapor mixing ratio, since we consider that liquid water will precipitate.

$$\frac{\partial(pq)}{\partial t}+\nabla.(pq\,\vec{v})=-\frac{\partial(pq\dot{s})}{\partial s}-pC_q \qquad (3.5b)$$

where again π is π_{trop} or π_{strat} as with the equation for θ.?

The momentum equation, for layers within the PBL, is

$$\frac{\partial \vec{v}}{\partial t} + \vec{v}.\nabla\vec{v} + f\vec{k}\times\vec{v} = -\nabla_p \Phi - \dot{s}\frac{\partial \vec{v}}{\partial t} + \frac{1}{r}\frac{\partial F_v}{\partial z} \qquad (3.6a)$$

where the last term is the vertical convergence of the turbulent flux of momentum. This term is discussed in section 3. In the free atmosphere, the momentum equation is

$$. \frac{\partial \vec{v}}{\partial t} + \vec{v}.\nabla\vec{v} + f\vec{k}\times\vec{v} = -\nabla_p \Phi - \dot{s}\frac{\partial \vec{v}}{\partial t} \qquad (3.6b)$$

The geopotential $\phi = gz$ is diagnosed from the hydrostatic equation, $\delta\Phi = -\theta\delta\Pi$.

2.2 Discrete equations

We discuss next the vertical discretization of the governing equations within the PBL. Discussion for the free atmosphere is found in the class notes of AS xxx course.

The atmosphere is vertically divided into layers (Fig. 2), from k = 1 (uppermost layer) to k = M (lowermost layer). We use half integer indices for labeling the layer interfaces; k+1/2 is the interface between layer k and layer k+1. The top of the atmosphere is the first layer interface, with vertical index 1/2, and the Earth surface is the last layer interface, with vertical index M+1/2. The lowermost free atmosphere layer has vertical index L, and uppermost PBL layer has vertical index L +1. The interface between these two layers is the PBL top, defined as level B with vertical index L+1/2. For $p = p_B, \sigma = \sigma_B = 1$ and for $p = p_S, \sigma = \sigma_S = 2$.

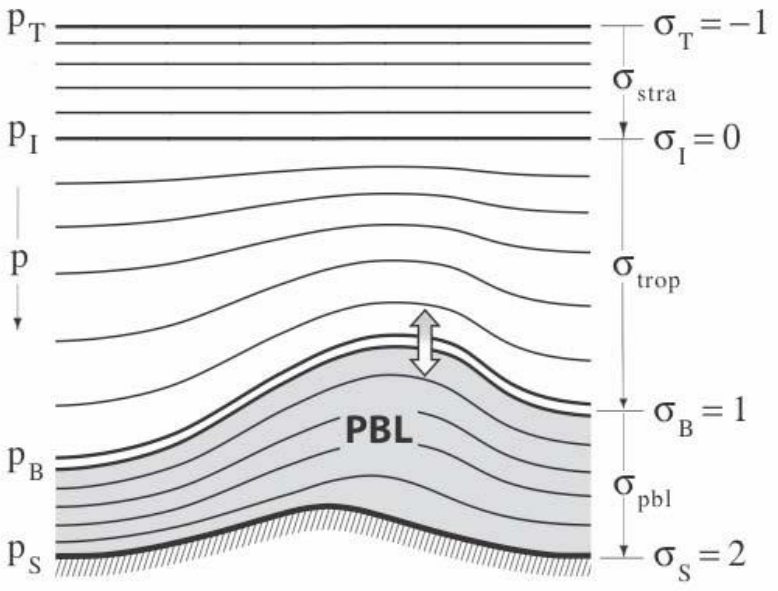

FIG. 2. Vertical structure and sigma coordinate of the UCLA-AGCM.

Horizontal velocity, temperature and water vapor mixing ratio are predicted for the layers, while vertical velocities ($D\sigma/Dt$) are computed at the layer interfaces.

We discretize the mass continuity equation by

$$\frac{\partial p}{\partial t} = -\nabla.(p\vec{v})_k - \frac{1}{(ds)_k}\left[(p\dot{s})_{k+1/2} - (p\dot{s})_{k-1/2}\right] \tag{3.7}$$

where k=1,2,..M, π is π_{PBL}, π_{trop} or π_{strat}, according to the vertical interval in which the layer is, and $(\delta\sigma)_k \equiv \sigma_{k+1/2} - \sigma_{k-1/2}$.

At the interface between the PBL and the free atmosphere, we compute the vertical mass flux as

$$(p_{PBL}\dot{s})_{L+1/2} \equiv (p_{PBL}\dot{s})_B \equiv -g(E - D - M_B) \tag{3.8}$$

where we take E > 0 if there is mass entrainment into the PBL, or D > 0 if there is mass detrainment from the PBL (D=-E). M_B is the cumulus mass detrained from the PBL to the cumulus clouds through their bases. Total or partial summation of equation 3.7 in the

vertical indexes allows for prediction of p_s, π_{PBL}, π_{trop} and π_{strat} and also for diagnose $\dot{ps}$ at any interface between layers (here we focus on PBL interfaces). Summation of equation 3.7 from k=1 to k=M, considering that $\dot{ps} = 0$ for k=1 and k=M, yields a prognostic equation for p_s:

$$\frac{\partial p_S}{\partial t} = -\sum_{K=1}^{Kstrat} \nabla.(p_{strat}\vec{v})(ds)_k - \sum_{kstrat+1}^{L} \nabla.(p_{trop}\vec{v})(ds)_k - \sum_{K=L+1}^{M} \nabla.(p_{PBL}\vec{v})(ds)_k \qquad (3.9)$$

summation for all layers within the PBL and above PBL gives a prognostic equation for π_{PBL} and π_{trop}, respectively:

$$\frac{\partial p_{PBL}}{\partial t} = -\sum_{K=L+1}^{M} \nabla.(p_{PBL}\vec{v})(ds)_k + (p_{PBL}\dot{s})_B \qquad (3.10a)$$

$$\frac{\partial p_{trop}}{\partial t} = -\sum_{K=1}^{Kstrat} \nabla.(p_{strat}\vec{v})(ds)_k - \sum_{kstrat+1}^{L} \nabla.(p_{trop}\vec{v})(ds)_k - (p_{PBL}\dot{s})_B \qquad (3.10b)$$

Note that from p_s and π_{PBL} we obtain p_B. On the other hand, partial summation of 3.7 can also give the way of diagnose vertical velocity (in terms of sigma) in the interfaces within the PBL and above it. This quantity is necessary for vertical advections in prognostic equations of q (or r), θ and **v**.

Within the PBL vertical velocity in terms of σ can be computed from,

$$(p_{PBL}\dot{s})_{k+1/2} = \frac{(s_S - s_{k+1/2})}{(s_S - s_B)}(p_{PBL}\dot{s})_B + \frac{(s_{k+1/2} - s_B)}{(s_S - s_B)} \sum_{kstrat+1}^{L} \nabla.(p_{PBL}\vec{v})(ds)_k - \sum_{K=L+1}^{M} \nabla.(p_{PBL}\vec{v})(ds)_k$$

(3.11)

We next discus discuss discretization of vertical terms for θ and r prognostic equations. If ψ is either θ or r, in the uppermost PBL layer, L+1, which is between interfaces L+1/2, PBL top (B level), and L+3/2, we have

$$\left[\frac{\partial(p_{PBL}y)}{\partial t}\right]_{L+1} = \frac{1}{(ds)_{L+1}}\left[y^{ext}_{B}(p_{PBL}\dot{s})_{B} - y_{L+3/2}(p_{PBL}\dot{s})_{L+3/2}\right]$$
$$+\frac{g}{(ds)_{L+1}}\left(\overline{w'y'}\right)_{L+3/2} + contribution\ of\ \ horizontal\ l.\ scale\ \ flux. \qquad (3.12a)$$

In this expression turbulent flux $\left(\overline{w'y'}\right)_{L+3/2}$ is the one due to large scale eddies, and is computed as shown in section 2.1a. plus the one due to small scale eddies as defined in section 2.1b. These ones are computed for r, v and h as

$$\left(\overline{w'?'}\right)_{L+1/2\ small\ scale} \equiv 0$$
$$\left(\overline{w'?'}\right)_{m+1/2\ small\ scale} \equiv \frac{K_{m+1/2}}{(dz)_m}(?_{m+1} - ?_{m-1})\ \ with\ \ m = L+1,\ldots,M-1$$
$$\left(\overline{w'?'}\right)_{M+1/2\ small\ scale} \equiv 0$$

while for θ they are deduced from the small scale turbulent fluxes of h and r in an analogous way as discussed for the turbulent fluxes due to large scale eddies (equations 2.6 and 2.9). ψ^{ext} represent an extrapolation of ψ from the levels above the PBL if E>0 or from below PBL top if E<0 (D>0). This is therefore an "upstream scheme". Note that we don´t consider turbulent fluxes at the PBL top. This is understood if we consider that the equation is based on a budget for variable y at the L+1 layer, in this budget we consider the top border as the level B+.

For intermediate PBL layers, (k = L+2, …, M-1),

$$\left[\frac{\partial(p_{PBL}y)}{\partial t}\right]_{L+1} = \frac{1}{(ds)_{L+1}}\left[y_{k-1/2}(p_{PBL}\dot{s})_{k-1/2} - y_{k+1/2}(p_{PBL}\dot{s})_{k+1/2}\right]$$
$$+\frac{g}{(ds)_{L+1}}\left[\left(\overline{w'y'}\right)_{k+1/2} - \left(\overline{w'y'}\right)_{k-1/2}\right] + contribution\ of\ \ horizontal\ l.\ scale\ \ flux. \qquad (3.12b),$$

with k=L+1,…M-1. For the lowermost PBL layer, next to earth's surface, k=M, and

$$\left[\frac{\partial(p_{PBL}y)}{\partial t}\right]_M = \frac{1}{(ds)_M}\left[y_{M-1/2}(p_{PBL}\dot{s})_{M-1/2}\right] + \frac{g}{(ds)_M}\left[\left(\overline{w'y'}\right)_{M+1/2} - \left(\overline{w'y'}\right)_{M-1/2}\right] + \textit{contribution of horizontal l. scale flux.} \quad (3.12c)$$

Note that M+1/2 level corresponds to Earth's surface, and turbulent fluxes at this level are the Earth's surface fluxes obtained through equations 2.12. It can also be noted that equations 3.12 require some definition of ψ (θ or r) at half integer levels between L+3/2 and M-1/2 (layer interfaces). θ values are defined as in Arakawa Suarez (1983), while r values at these half integer levels are taken as the semi sum of the values at the adjacent layers.

The discretization of the vertical advection of momentum follows Arakawa and Lamb (1977). For the upper-most PBL layer,

$$\left(\dot{s}\frac{\partial\vec{v}}{\partial s}\right)_{L+1} \equiv \frac{1}{2p_{PBL}(ds)_{L+1}}\left[(\vec{v}_{L+2}-\vec{v}_{L+1})(p_{PBL}\dot{s})_{L+3/2} + (\vec{v}_{L+1}-\vec{v}_B)(p_{PBL}\dot{s})_B\right] \quad (3.13a)$$

The term $\vec{v}_B(p_{PBL}\dot{s})_B$ is computed with an upstream scheme as before.

For the intermediate PBL layers,

$$\left(\dot{s}\frac{\partial\vec{v}}{\partial s}\right)_k \equiv \frac{1}{2p_{PBL}(ds)_k}\left[(\vec{v}_{k+1}-\vec{v}_k)(p_{PBL}\dot{s})_{k+1/2} + (\vec{v}_k-\vec{v}_{k-1})(p_{PBL}\dot{s})_{k-1/2}\right] \quad (3.13b)$$

with k=L+2,….M-1. For the lower-most PBL layer,

$$\left(\dot{s}\frac{\partial\vec{v}}{\partial s}\right)_M \equiv \frac{1}{2p_{PBL}(ds)_M}\left[(\vec{v}_M-\vec{v}_{M-1})(p_{PBL}\dot{s})_{M-1/2}\right] \quad (3.13c)$$

The geopotential used in the momentum equation is computed with the discrete form of the hydrostatic equation discussed in Arakawa Suarez (1983).

4- Selected results of the AGCM with the new PBL scheme

The PBL parameterization described in Section 2 was incorporated into the UCLA AGCM. To illustrate the performance of the revised model, we have carried out simulations in an uncoupled mode with prescribed sea surface temperatures (SST). These simulations are 5-year long and use the low-resolution version of the AGCM, which is 5^o long. by 4^o lat. with 18 layers (4 in the PBL). The initial condition corresponds to November 30 in a long-term run of a previous model's version with the same resolution, but using a single-layer PBL. The SST, sea-ice, Earth's surface albedo and roughness, and ground wetness distributions are obtained daily by linear interpolation from the twelve monthly means of observed climatologies taken from the Global Sea-Ice and SST Data Set (Rayner et al. 1995) for SST, and Dorman and Sellers (1989). We show averages of monthly means over the 5-year period, and hourly outputs of PBL variables. Our emphasis in this section is on surface fields, which are most directly impacted by the PBL scheme.

a) Global surface fields

We start by looking at the simulated monthly-mean sea level pressure. Figure 3 shows the observed distributions for January (a) and July (c) from the NCEP reanalysis (Kalnay et al. 1996), and the simulated ones (b, d). The simulation reproduces clearly the main features of the observed climatology, such as the subtropical highs in the Northern Hemisphere during summer, the Aleutian low during winter, and the subtropical highs in the Southern Hemisphere both in winter and summer, In January, the simulated sea level pressure over the continents in the Northern Hemisphere tends to be lower than in the

NCEP reanalysis. Note that differences between the observation and simulation over Tibetan plateau are influenced by the method used to obtain values at sea level in regions of high terrain. The simulated a low pressure belt around Antarctica low pressure belt around Antarctica is too weak in both January and July, which is feature fairly common to AGCMs with low resolutio n (Boville 1991).

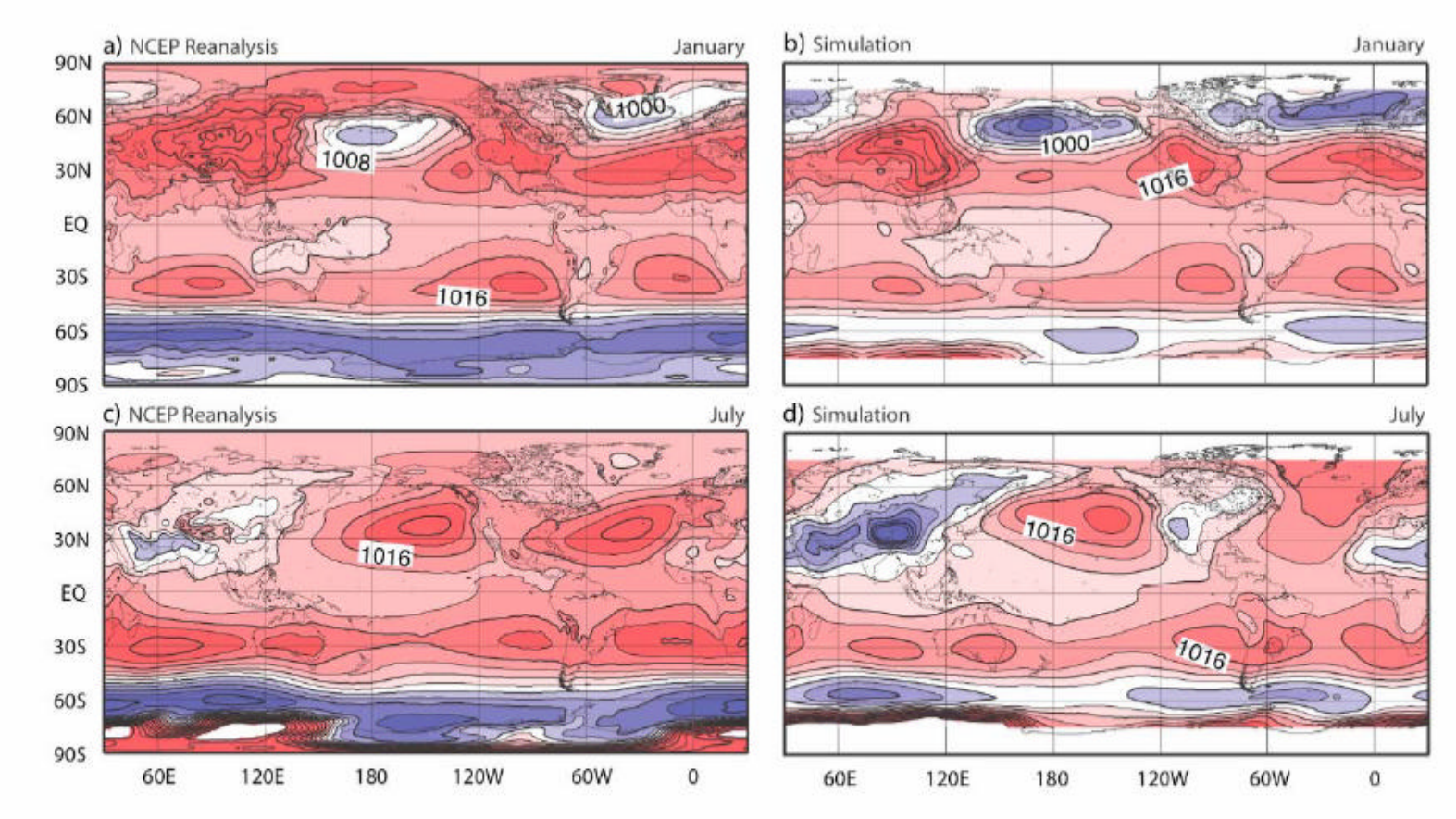

FIG. 3. Sea level pressure (hPa, SLP) from NCEP reanalysis (left column) and simulations (right column) for January (upper row) and July (lower row). Contour interval is 4 hPa.

Figure 4 shows the simulated monthly-mean PBL depth, TKE and stratocumulus clouds incidence (as percentage of time of occurrence) for January, April, July and October. PBL depth (left column) is generally lower over the continents than over the oceans. This is due to the strong diurnal cycle of PBL over land, with very shallow PBLs during night-time over cold ground, although PBLs can be very deep during day-time as solar radiation warms the surface. Over the oceans there are local maxima along the major storm tracks, particularly during winter. PBLs tend to be deep in the subtropical and tropical regions with high incidence of marine stratocumulus clouds. In the western tropical oceans, cumulus activity prevents PBL from becoming to deep. TKE (central column) over the oceans has local maxima at locations that approximately coincide with those of larger PBL depth and stratocumulus incidence (right column). Over the continents local maxima of TKE tend to be in regions with either convectively unstable PBL regime during daytime, or with high low-level winds over rough surface (not shown). The geographic distribution and seasonal cycle of simulated stratocumulus clouds are consistent with the observation (e.g., Klein and Hartmann 1993). The eastern parts of the subtropical oceans show high stratocumulus incidence that characterizes the climate of those regions. In the northeastern Pacific, stratocumulus incidence is maximum in July,and minimum in January (Fig. 4*i* and 4*k*). In the southeastern Pacific and Atlantic, the maximum is in October and the minimum in April (Fig. 4*j* and 4*l*). The simulation also shows high stratocumulus incidence along the major storm tracks, this feature is consistent with the climatology of Klein and Hartmann (1993).

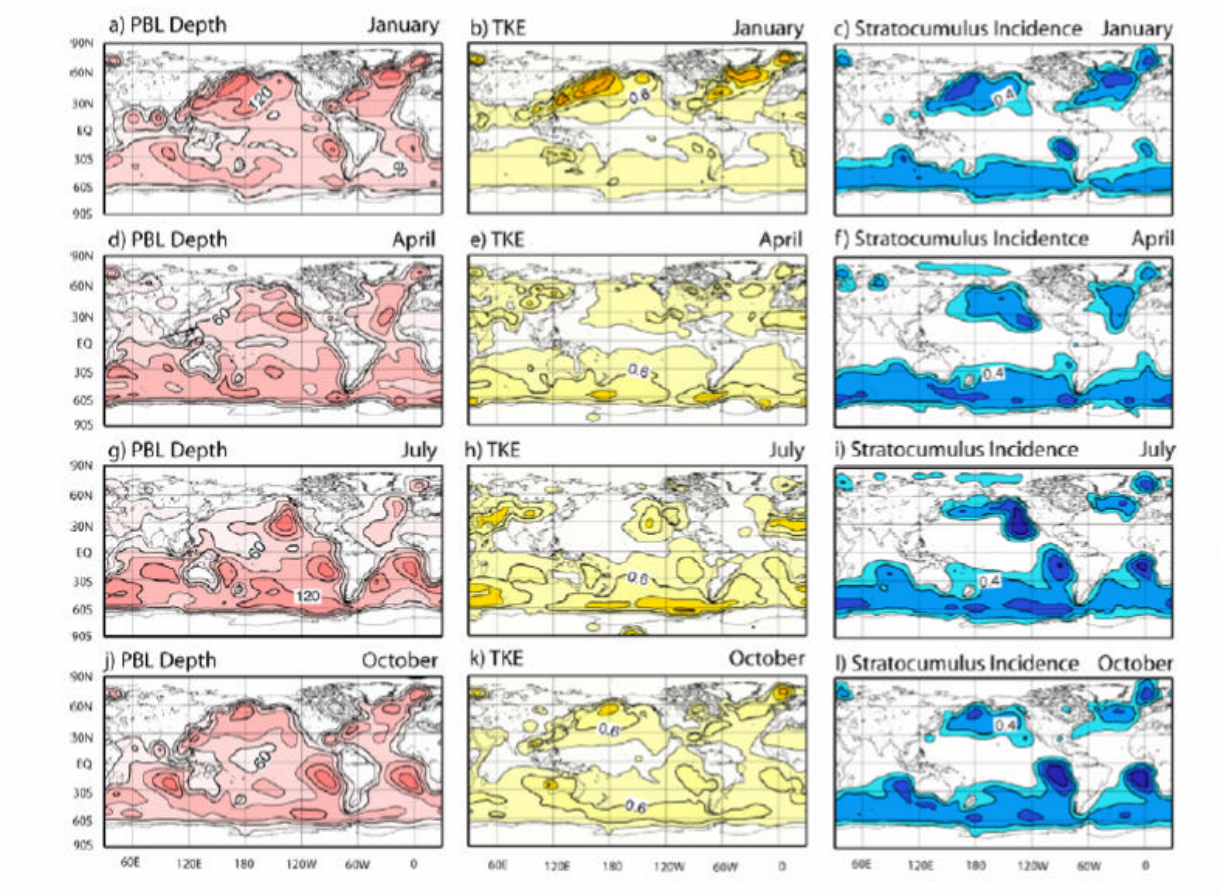

FIG. 4. Monthly-mean PBL-depth (hPa, with 30 hPa contour interval, left column), TKE ($m^2 s^{-2}$, with 0.2 $m^2 s^{-2}$ contour intervals, middle column) and stratocumulus incidence (with 0.2 contour interval, right column) for January (uppermost row), April (second from top), July (third from top) and October (lowermost row).

The approximate collocation over the oceans of larger values in PBL depth, TKE, and stratocumulus incidence suggests the interdependence between these variables. The results obtained fit the following scenario. Higher values of TKE tend to produce deeper PBLs, which favors higher stratocumulus incidence. In turn, higher radiative cooling associated with stratocumulus tends to increase TKE, which sets up a positive feedback. These aspects are further discussed in section 4.

The next concentrate on the surface fluxes of heat and water vapor. Latent heat flux, which is also strongly tied to PBL processes, provides contributions to the net after that of short wave radiation over the tropical and subtropical oceans. Figure 5 shows the observeded upward latent heat flux from COADS analysis (Da Silva et al. 1994) averaged from 1979 to 1993 for January (a), July (c), and the corresponding simulated fields ((b) and (d), respectively). In general, the simulation reproduces the observed patterns reasonably well. For example, the relatively large values tend to occur over the subtropical oceans of the winter hemisphere. In January, the strong fluxes from the Kuroshio current and the Gulf Stream are well captured. The simulated values of the subtropical part are to strong at spots in the Bay of Bengal and off the Pacific coast of Central America, and in the central part of the subtropical North Atlantic. Otherwise, differences (nor shown) between simulation and analysis are generally one order of magnitude smaller than the actual fields. In July, the simulated latent heat flux distribution compares reasonably well with the observed one.

The net solar radiation flux is the most important contribution to the heat flux into the ocean, and the PBL clouds directly affects its values. Figure 6 shows the monthly-mean fields for January and July (c) form NASA SRB Analysis (http://srb-

swlw.larc.nasa.gov/GEWEX_SRB_homepage.html) averaged from 1983 to 1991 (left column, upper and lower panels respectively) and from the simulation (right column, upper and lower panels respectively). A comparison of Figs. 6a to 6b shows that the simulation reproduces the observed pattern reasonably well for January, except that the amplitude of simulated values tend to be too large over the Indian Ocean. For July, simulations (Fig. 6d) tend to yield larger values than observation (Fig. 6c) off the coasts of California and Peru where the simulated incidence of stratocumulus is high (see Fig. 4i). This may indicate that the stratocumulus appear more transparent that they should be to the radiation parameterization in the model. This is one of the issues that we will address in our future versions. ? ? ?

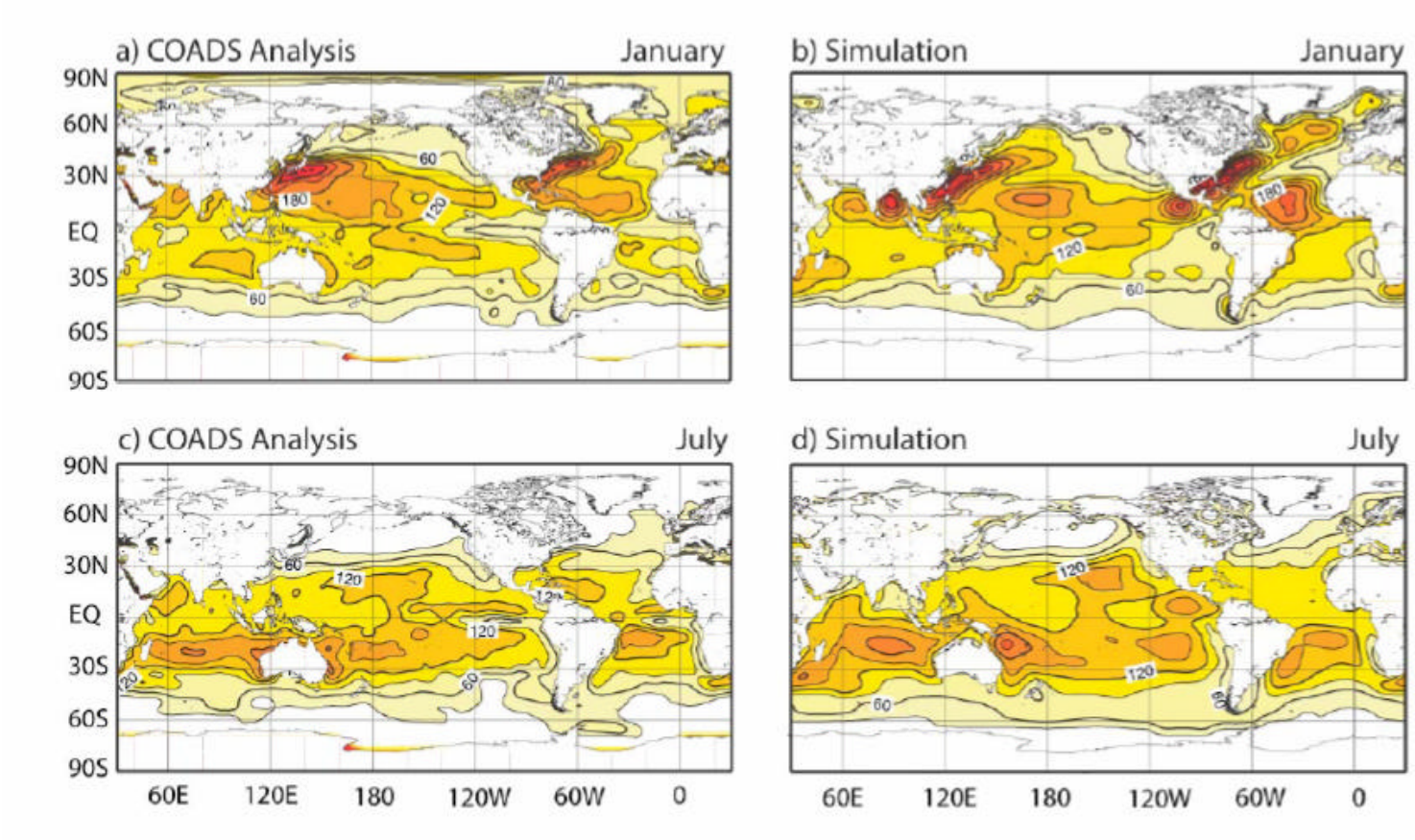

FIG. 5. Latent heat flux (Wm^{-2}) at the surface from the COADS analysis (left column) and simulations (right column) for January (upper row) and July (lower row). Upward flux is positive with 30 Wm^{-2} contour intervals.

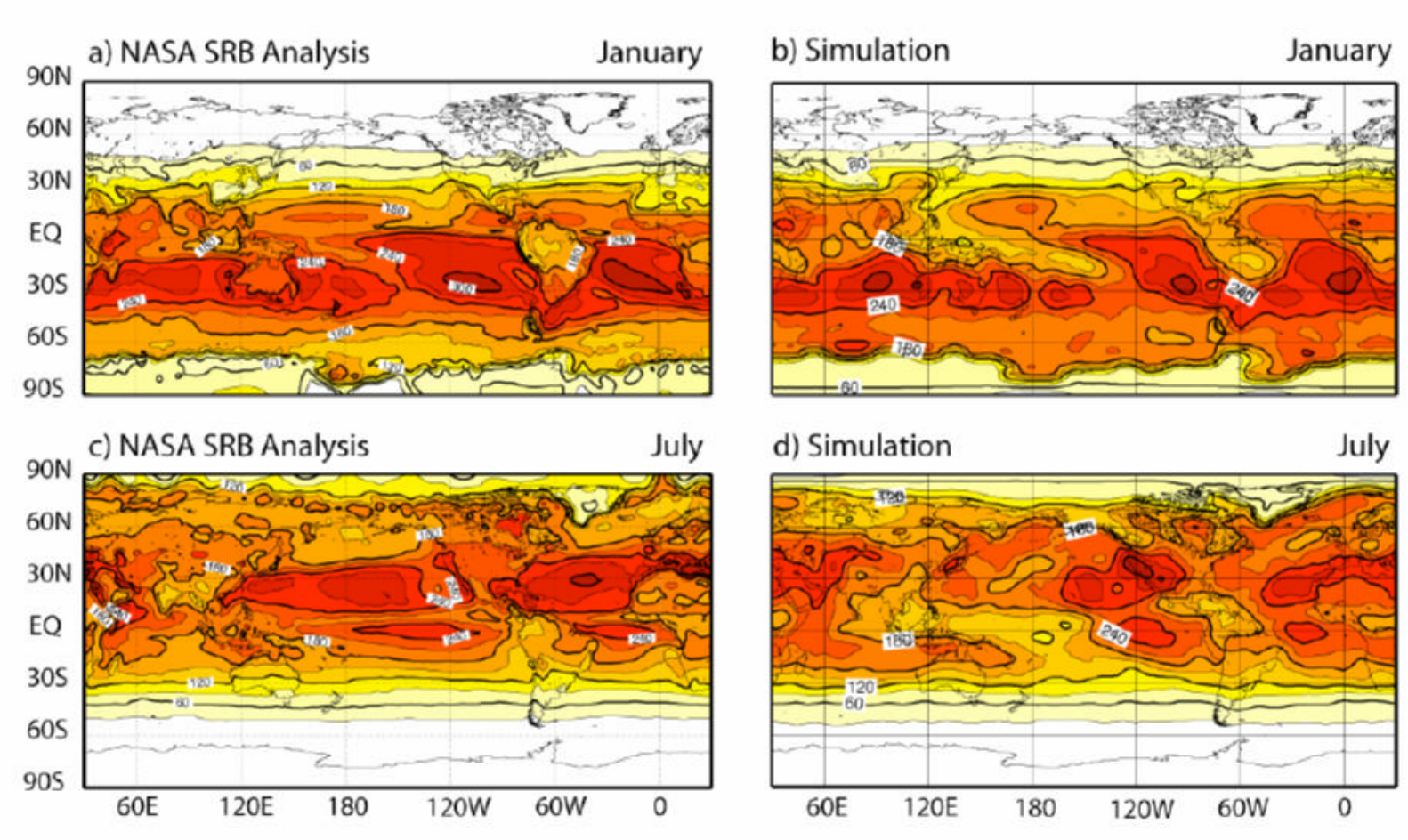

FIG. 6. Net short wave radiation flux (Wm^{-2}) at the surface from the NASA SRB analysis (left column) and simulations (right column) for January (upper row) and July (lower row). Downward flux is positive with 30 Wm^{-2} contour intervals.

b) Vertical Profiles of Thermodynamic Variables over Ocean

Figure 7 shows instantaneous vertical profiles of moist static energy, potential temperature and total water, water vapor and liquid water mixing ratios, simulated at 125W-30N. The location corresponds to the region of the DYCOMS II field study (Stevens et al. 2002), which provided observational estimates of those profiles. The profiles in Fig. 7 correspond to July 25 of the first simulated year at three different local times: 06:00 (solid lines), 18:00, and next 6:00 (dotted). The moist static energy and total water mixing ratio profiles show that these variables are well mixed in the vertical are well mixed in the vertical. This is a reasonable feature for a convectively active PBL and is consistent with DYCOMS profiles. The potential temperature increases and water vapor mixing ratio decreases with height above the condensation level, and are nearly constant below that level. condensation level and increases with height above that level. The multilayer PBL formulation, therefore, can capture the departure from well-mixed profiles of those variables in the cvloud layer, as well as the near-constancy of these quantities in other layers. It should be noted, however, that the daily mean liquid-water content simulated by the model appears higher than the DYCOMS II observation.

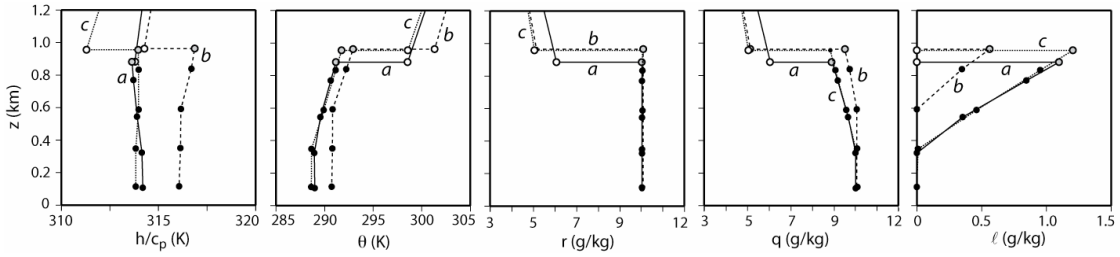

FIG. 7. Vertical profiles of moist static energy (left), potential temperature (second from left), total water mixing ratio (middle), water vapor mixing ratio (second from right) and liquid water mixing ratio (right).

This is another issue that we will address in our future revisions.

The simulated diurnal variation of stratocumulus properties is weaker than the observed (e.g. Duynkerke and Hignett 1993). This is partially due to the missing link between the short wave radiation, entrainment and TKE in the current formulation, which will be further discussed in the next chapter. Thus, the depth of cloud-topped PBL does not show a visible diurnal variation. Nevertheless, there is a clear diurnal variation in temperature, and consequently, in cloud base height since the solar short wave radiation warms the cloud air in the day time.

c) Behavior of PBL over Land

In this subsection, we focus on January (austral summer) and select two locations over land corresponding to moist and semi-arid soil. On these locations, therefore, we expect PBL turbulence to be well developed during daytime. Figure 8 shows the mean diurnal over five Januarys simulated at the location in the Amazon basin (60^{o}W-10^{o}S) of PBL thickness (a), ground temperature (b), TKE (c), precipitation (d), latent and sensible heat fluxes from the surface (e), and short and long wave radiation fluxes into the surface (f). The precipitation peaks in the early afternoon, consistently with observations during the warm season at nearby locations (Machado et al. 2002, Lin et al. 2000, Bastable et al. 1993). The amplitude of the simulated diurnal cycle of ground temperature is about 6 K, which is similar to the one found in the observations of air temperature close to the ground (e.g., Lin et al. 2000; Bastable et al. 1993). The simulated diurnal cycles of latent, sensible and radiation heat fluxes shown in Figs. 6e and 6f are also comparable with the observations reported by the same authors. We note that latent heat flux is much stronger than sensible heat flux. During morning hours, short wave radiation heating prevails over

cooling by latent heat and long wave flux, causing the ground temperature to rise. During the late afternoon, cooling effects prevail and temperature decreases. During night hours, the upward long wave radiation and downward sensible heat fluxes tend to balance at the surface.

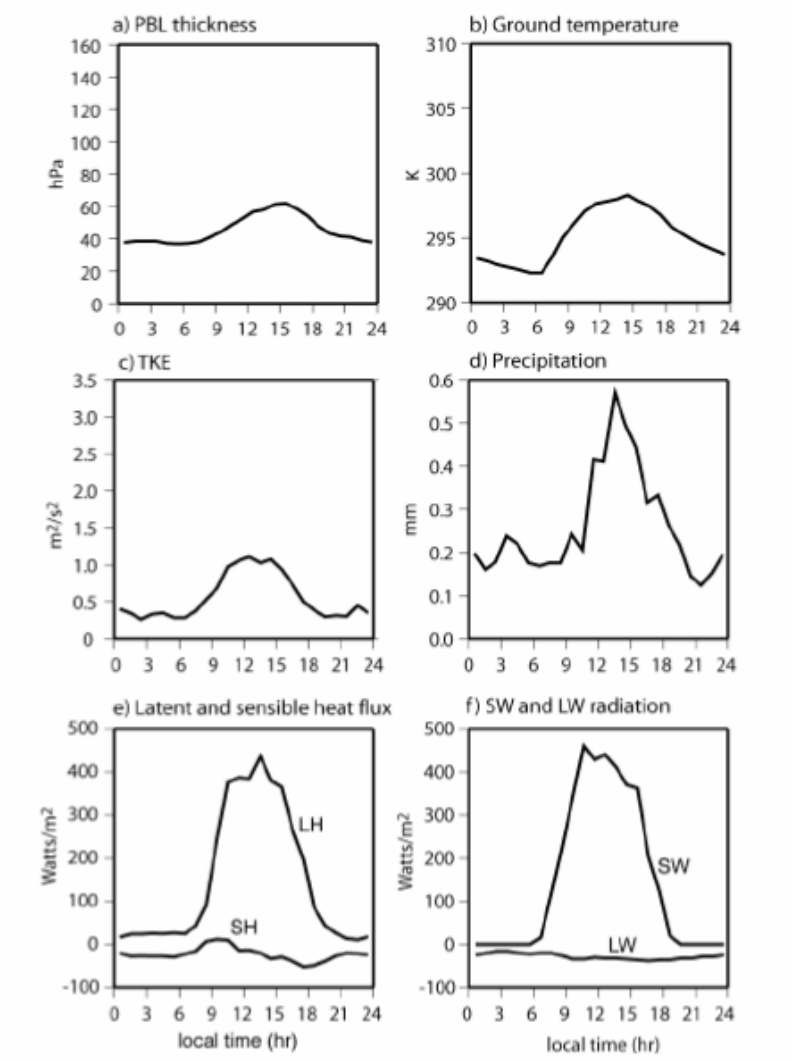

FIG. 8. Mean diurnal cycles at 60W-10S for January of (a) PBL thickness, (b) ground temperature, (c) TKE, (d) hourly precipitation rate, (e) upward latent and sensible heat flux at Earth's surface (curves indicated with "LH" and "SH", respectively) and (f) downward short and long wave radiation fluxes at Earth's surface (the curves indicated with "SW" and "LW", respectively). The diurnal cycles are given as function of local time.

Figure 9 shows the same composite diurnal cycles as Fig. 6, except for the location in Australia (135^{o}E-26^{o}S). The amplitudes of the diurnal cycle of PBL thickness, ground temperature, TKE, and short and long wave radiation fluxes are stronger than at the location in the Amazon basin. Also, sensible heat flux provides a relatively more important contribution to the net.

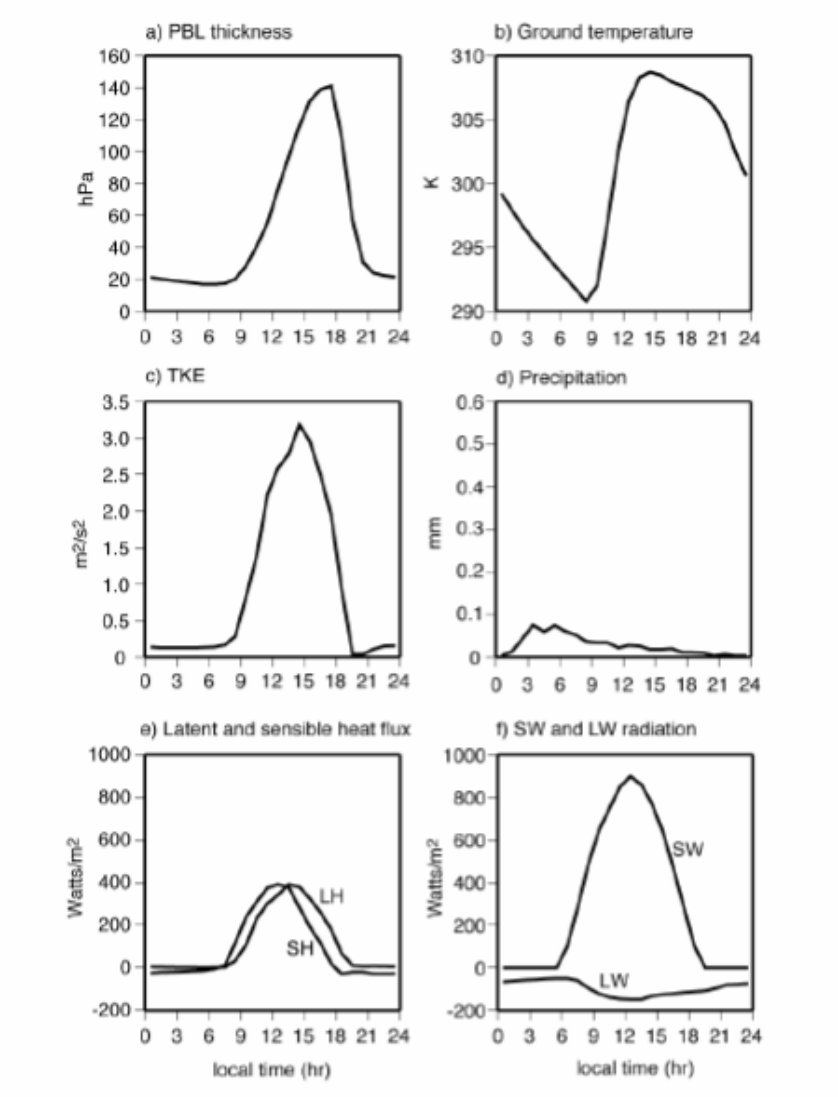

FIG. 9. Same as Fig. 8, except at 135W-26S

Precipitation in the Australia location, (d) is generally much smaller than at the Amazon basin location, with a weak maximum by early morning. The contribution of cumulus convection to total precipitation is negligible. During night hours the PBL becomes very shallow. During daytime hours, the high sensible heat flux from the ground contributes to an increase of TKE and PBL thickness.

d) Comparison of the AGCM performance with the new and previous PBL parameterizations.

To asses the impact of the new scheme, we compare the simulation described in the previous subsections with another that uses the previous version of the PBL parameterization (hereafter SP simulation). The reader is referred to Suarez et al. (1983) for a detailed description of the previous version. In short, the previous parameterization treats the PBL as a well-mixed single layer, the entrainment rate is determined by solving an implicit equation, and the aerodynamic formulas to determine the surface fluxes use the mean PBL wind as velocity scale. The implicit equation that determines the entrainment rate is obtained by neglecting the time derivative term in the TKE budget equation similar to (2). A complex iteration procedure discussed by Suarez et al. (1983) is used to solve the resulting equation for the entrainment rate. This parameterization has two potential shortcomings in comparison to the new, first of which is that neglecting the time derivative of TKE in the TKE budget eliminated the transient behavior of PBL. The second is that there is no room to directly implement physical processes for entrainment beyond the equilibrium of TKE.

Figure 10 shows the January and July-mean PBL depth (a and b, respectively) and stratocumulus incident (ca and d, respectively) in the SP simulation. A comparison with

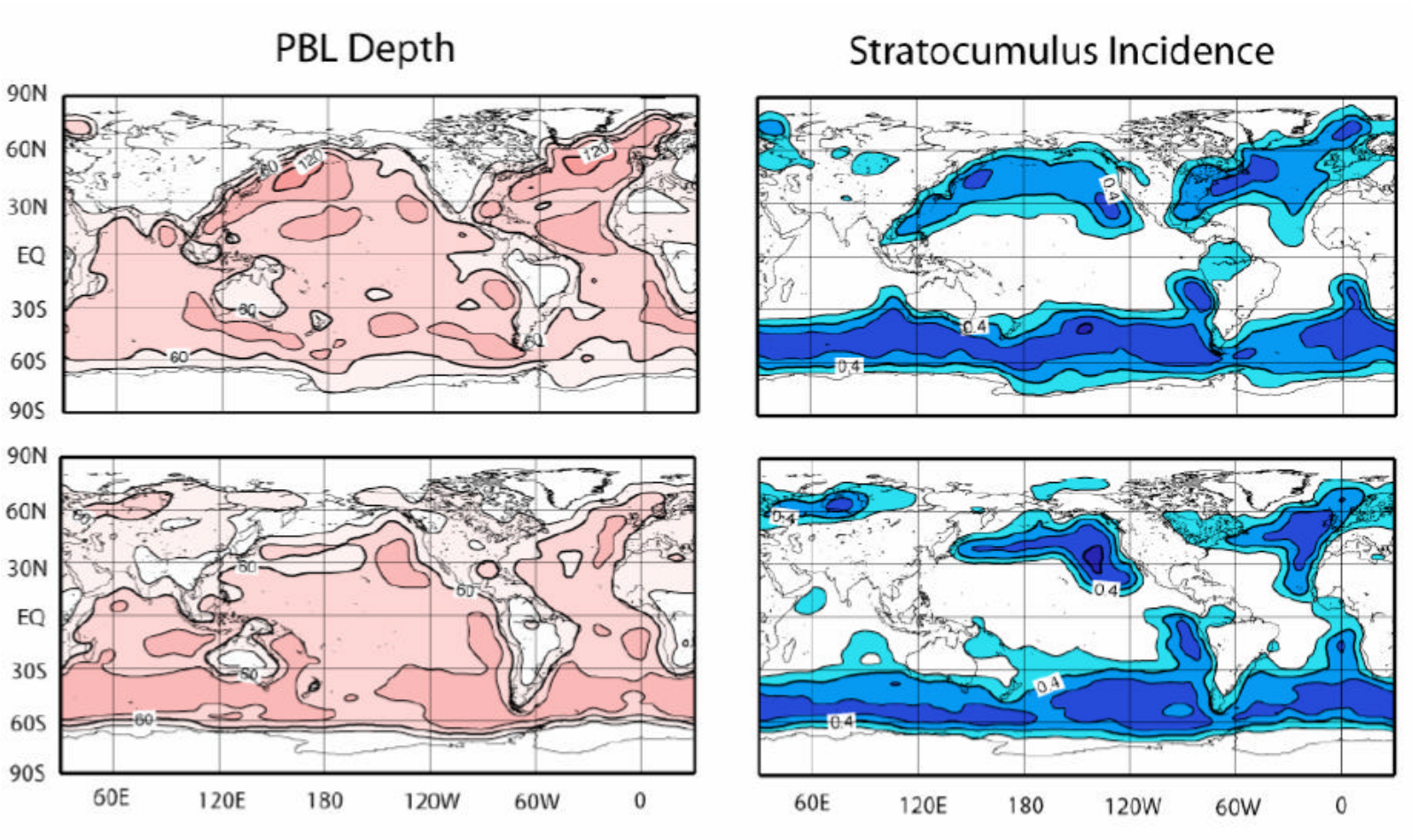

FIG. 10. Same as relevant panels of Fig.4, except for the SP simulation.

Control (Fig. 4) shows that the new parameterization generates more detailed PBL patterns (Fig 4a for January and g for July) and a better seasonal variability of stratocumulus incidence (Fig. 4c for January and i for July), particularly in the stratocumulus regions. Fig. 11 shows the January- and July-mean net latent heat fluxes at the surface in the SP simulation. Overall, upward fluxes in SP simulation are larger than in the observation (Fig. 5a for January and c for July) and Vcontrol (Fig. 5b for January and d for July). The overall pattern of the fluxes in the southern Tropics in July is less zonal than the observation and Control. Over the eastern Pacific, however, the new formulation gives higher values than the observation and SP simulation. The monthly-mean net shortwave radiation fluxes at the surface for the same months in the SP simulation (Fig. 12a and 12b) compares reasonably well with both the observed (Fig. 6a and c) and Control (Fig. 6b and d). There is, nevertheless, a small improvement with the new parameterization over the Southern Hemisphere Atlantic and Pacific Oceans in January. It is clear from these comparisons that the new PBL parameterization has overall significantly improved the estimation of the surface latent heat flux in our GCM. Moderate to small improvements are also achieved in the simulation of seasonal variability of stratocumulus incidence and the estimates of net shortwave radiation flux at the surface. We attribute a large part of these improvements to the explicit prediction of TKE and its use in the determination of entrainment rate and surface fluxes in the new PBL parameterization. The overall improvement of the simulated surface latent heat fluxes with the new parameterization is primarily due to the use of the square root of TKE as a velocity scale in the aerodynamical formula for the surface flux. Particularly in the Tropics, where the mean PBL wind is weak, the surface fluxes are controlled by the

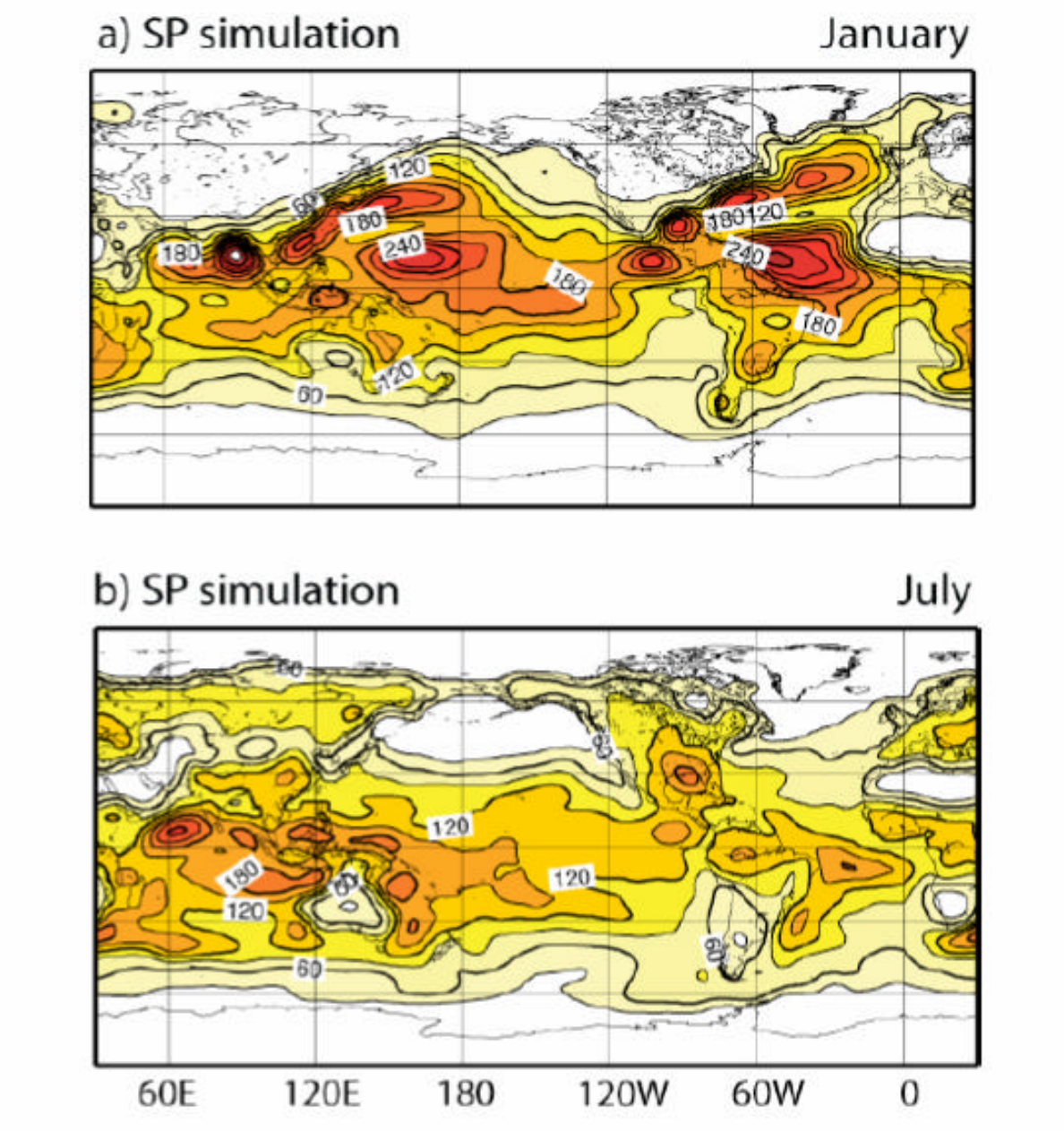

FIG. 11. Same as Fig.5, except for the SP simulation

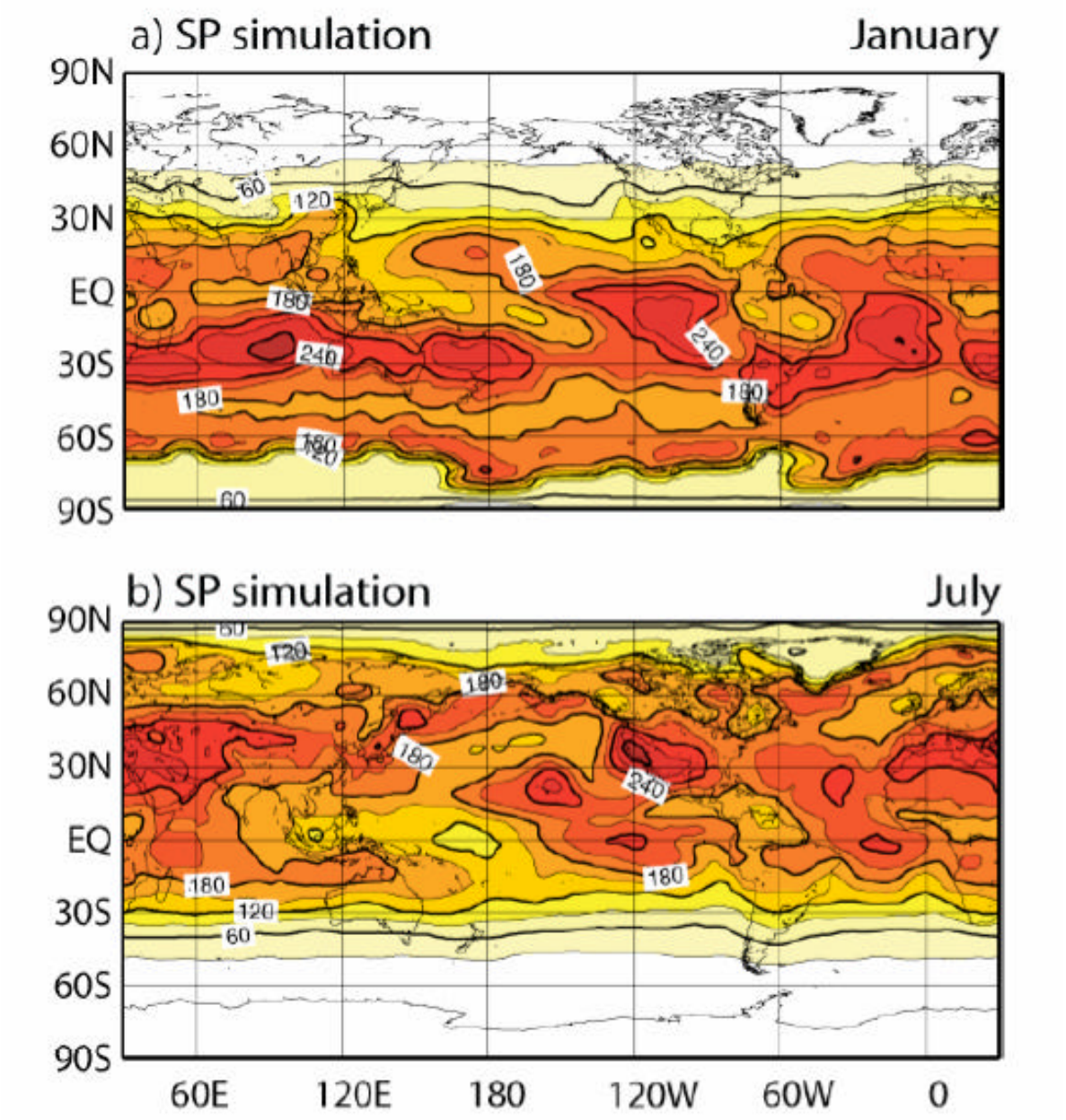

FIG. 12. Same as Fig.6, except for the SP simulation.

sub-grid scale convective activity, which is well represented by the bulk TKE.

e. Comparisson of simulated baroclinic activity with a multi- and single-layer PBL parameterizations.

In the introduction we sated that explicit prediction of vertical shears within the PBL could have an impact on the evolution of extratropical baroclinic disturbances. To examine this potential impact we select the poleward heat transport near the surface (i. e., within the PBL) in synoptic scales as a proxy for baroclinic eddy activity. Then, we compare the values for our baroclinic activity to the one obtained by a version of the same AGCM, in which the number of layer for the PBL is set to one. Otherwise, these two versions of the model are identical.

Figure 13 shows the mean January (upper panel, a and b) and July (lower panel, c and d) latitudinal poleward potential temperature flux by eddies (v'q') within the PBL, where prime indicates deviation from the zonal mean, from the CONTROL (left column) and the single-layer simulation (right column). (The values for the CONTRO correspond to vertical averages within the PBL.) To focus on the synoptic scale baroclinic activity, a band-pass filter between 3 and 8 days is applied. A comparison of the panels (a) and © to (b) and (d) of Fig. 13, respectively, indicates that the multi-layer scheme generally yields higher baroclinic activity implied by the magnitude of (v'q') than the single-layer scheme does. It should be noted that the horizontal resolutions we are using are insufficient to properly resolve the details of synoptic scale eddies. Nevertheless, our comparison still indicates that the use of multiple layers in the PBL produces a more realistic level of baroclinic activity.

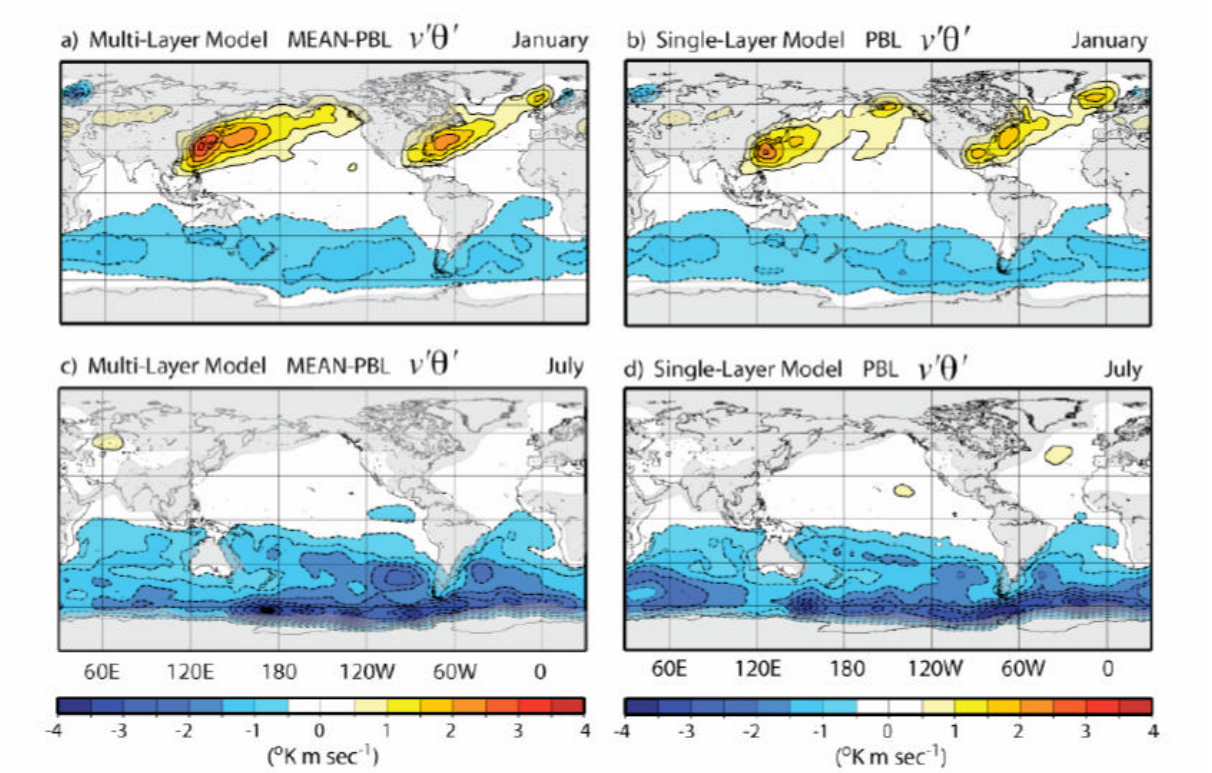

FIG. 13. Monthly-mean longitudinal potential temperature flux by eddies ($_0$Kmsec^{-1}). Upper and lower panels are for January and July, respectively. Left and right columns show results from the multi-layer CONTROL and single-layer simulation, respectively.

f. Performance of the AGCM coupled to an OGCM.

We have also performed simulations in which the AGCM coupled to a near global MIT-OGCM. (The reader is referred to Cazes-Boezio et al. (2005) for the coupled model results.) Experiments

in the coupled mode is a necessary task to validate AGCMs since prescribing SSTs in the uncoupled mode assumes the most important part of the answer and, therefore, it may hide crucial deficiencies of the model.

In the coupled simulations, the SST field (not shown) demonstrates several realistic features both in terms of annual means (such as realistic equatorial SST gradients in both

Pacific and Atlantic basins) and interannual variability (such as ENSO-like anomalies in SST and the atmospheric circulation). The

outstandingly successful feature f the simulations is that the extent and seasonal cycle of stratocumulus clouds and their effects on short wave radiation and SST in the eastern part of the subtropical oceans is well simulated. We attribute a large part of this success to the merits of our PBL framework.

5. Effects concentrated near PBL top

In this section we examine the importance of radiation, turbulence and thermodynamics interactions in the PBL when a startocumulus clouds are present. The radiative cooling at the PBL top is of fundamental importance for the generation of TKE and turbulence fluxes in a cloud-topped PBL. In the formulation we are presenting here, the PBL top coincides with that of stratocumulus clouds. Hence, the radiation calculation in the AGCM directly gives the value of radiative cooling at the PBL top, which is then explicitly used in the formulations the TKE generation, PBL top mass entrainment and the time derivative of potential temperature of the uppermost PBL layer. In our model, therefore, the importance of this cooling can easily be assessed by an experiment in which this effect is neglected.

We focus on July, during which the high incidence of startocumulus in the eastern parts of tropical and subtropical oceans is generally well captured by the AGCM (see Fig. 2). We start by performing a simulation in which radiative cooling at the PBL top is ser to zero in the calculation of TKE and mass entrainment, but kept in the potential temperature prediction (hereafter “NR1 simulation”). Note that the radiative cooling affects the TKE budget through the buoyancy generation as discussed in subsection 2b.

Figure 14 shows TKE, PBL depth and stratocumulus incidence from the NR1 simulation (Fig. 14a, c and e respectively) and the NR1 minus CONTROL differences. (Figs. 14 14b, d and f). In the eastern part of the subtropical and tropical oceans, regions in which stratocumulus incidence obtained in the Control is high, the PBL depth, TKE and stratocumulus incidence are reduced in the NR1 simulation. Off the coast of California, the reduction is as high as 60%, while off the coasts of Peru and Namibia the reduction is as about 30%. The lack of radiative cooling effect at the PBL top reduces the TKE and entrainment rate in the stratocumulus region, and thus PBL becomes shallower. A positive feedback is established as the PBL top lowers and condensation level rises. Along the North Pacific storm track, both NR1 simulations and CONTROL show a very shallow PBL (Figs. 4g and 14c), low TKE, and high stratocumulus incidence (Figs. 4i and 14e). In this region, PBL is usually stable. In such a situation, the lower entrainment rate produces higher incidence of fog since the mixing of air between the PBL and the overlying drier free atmosphere is reduced.

Despite the lower incidence of stratocumulus clouds in the eastern parts of subtropical and tropical regions in the NR1 simulation, there are still local maxima of PBL depth in these regions. This is partially due to the TKE generation by the upward surface heat fluxes resulting from low-level cold advection from higher latitudes along the eastern branch of the subtropical anticyclones. In addition, the radiative cooling of the cloud layer is still active in the NR1 simulation.

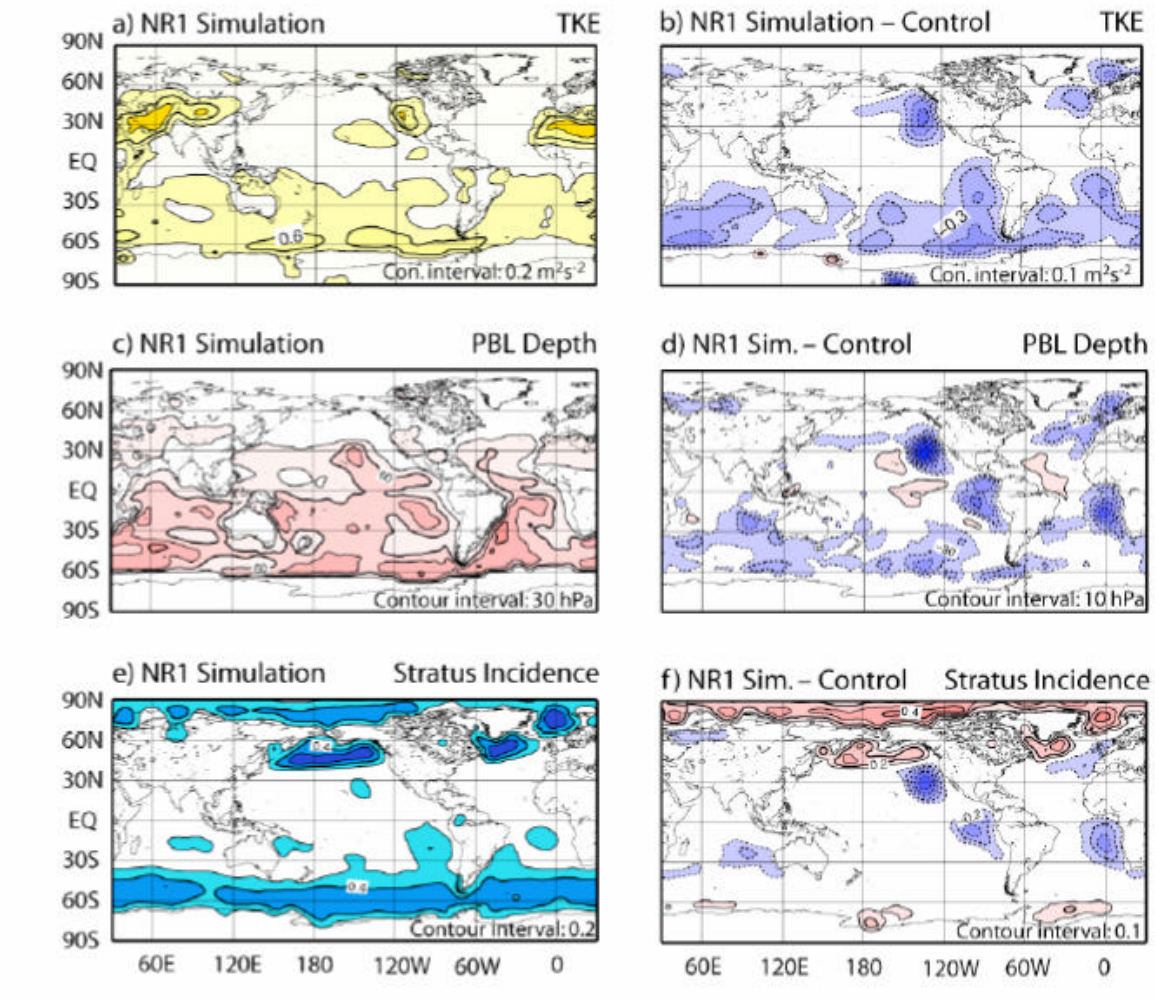

FIG. 14. Monthly-mean TKE (upper panel), PBL thickness (hPa, middle panel) and stratus incidence (lower panel) from the simulation with no radiative cooling effect in TKE and entrainment (NR1, left column) and difference between NR1 and Control (Fig. 4) simulations (right column).

To completely eliminate the effects of radiative cooling that influences the PBL, we set the radiative cooling to zero both in the calculation of TKE and mass entrainment and in the potential temperature prediction in the uppermost PBL layer. We call this experiment NR2. In this experiment, the stratocumulus incidence for July (see Fig. 15) is

further reduced from the NR1 simulation (Fig. 14) to the point of almost vanishing even in the regions where they are most persistent in the CONTROL (Fig. 4).

A comparison f the results of NR1 and NR2 experiments reveals that the cooling of the PBL air due to the cloud-top radiative cooling indirectly contributes to the budget of TKE (and therefore entrainment rate= and helps, to a certain degree, maintenance of stratocumulus decks over oceans. The indirect link is through the enhanced surface heat fluxes (and, therefore, through the buoyancy contribution to TKE) caused by the cooler PBL air under the clouds. This indicates the existence of a feedback process between the PBL clouds and surface heat fluxes.

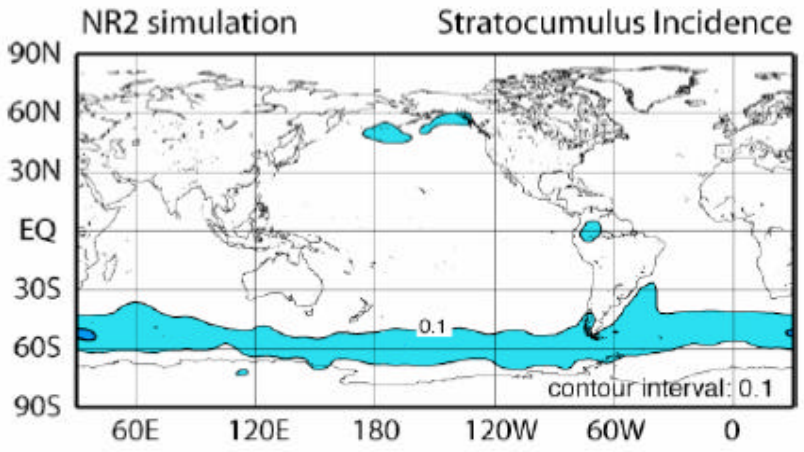

FIG. 15. Monthly-mean stratocumulus incidence from the simulation with no radiative cooling effect on TKE, entrainment and potential temperature for July (NR2 experiment).

6. Comparison with models with traditional vertical structures

In the previous section, we presented a comparison to assess the effect of processes associated with stratocumulus clouds on the turbulence fluxes using the new framework. To what degree the lack of these processes in a model with traditional PBL parameterization influences the simulation is an interesting question. There have been many studies that combine a traditional parameterization with interactive cloud parameterizations beyond diagnostic treatments (e. g. Soares el al. 2004, Lock et al. 2000). In this paper, however, what we mean with the traditional PBL parameterization is a parameterization characterized by two aspects. One is the "traditional" vertical structure, in which the vertical coordinate is a terrain following sigma type. As mentioned earlier, we use a different vertical structure, in which the PBL has its own multiple layers with predicted depth. In an early version of the UCLA AGCM, an attempt was made to incorporate a mixed-layer based PBL parameterization, with a traditional vertical structure (Randall, 1976). Not having the PBL top to coincide with a coordinate surface in the traditional vertical structure made the PBL -top jump very difficult to determine and caused the abandonment of this attempt later (Suarez et al. 1983). This experience is an indication that the vertical structure we use is paramount for a successful incorporation of the new PBL parameterization to our model. The second aspect of what we mean by the traditional parameterization is the use of diagnostically determined PBL clouds without formulation of their effects in the parameterization itself. We use such a parameterization to see the difference between prognostic and diagnostic determination of clouds in a simple context.

How the results obtained by a model with the traditional parameterization compare to those presented in section 3 is examined here. For this purpose we constructed a version of our model with the traditional vertical structure. To do that, first we replace the part of the vertical coordinate given by (1b) and (1c) for pi<p<ps by a conventional sigma coordinate such as the one defined as strop = Note that the total number of model layers is kept the same as in the CONTROL. For the PBL parameterization, we choose the scheme used by Holstlag and Boville (1993). The scheme requires a definistion of the PBL depth, for which we choose the diagnostic expression using a Bulk Richardson number intriduced by Troen and Mahrt (1986). In this experiment, we diagnose the PBL depth at each dynamics time step. To diagnose the PBL clouds, we calculated the lifting level of condensation (LLC). If the LLC is below the PBL-top height, it is assumed that the PBL is topped with stratocumulus clouds.

Figure 16 shows the July-mean distribution of the PBL depth, stratocumulus incidence diagnosed for the PBL and low-level cloud incidence simulated by this experiment, which we call the fixed-sigma simulation. The low-level cloud incidence (cloud incidence for the lowest 250 hPa deep portion of the troposphere) is presented because the stratocumulus clouds incidence diagnosed for the PBL may not fully represent the clouds resulted from the PBL processes in the fixed-sigma simulation. In the subtropical oceans, the distribution of maximum of the PBL depth distribution (Fig. 16a) are almost opposite to those in the CONTROL (Fig. 4g). In the fixed-sigma experiment, the regions of the observed high incidence of marine stratocumulus off the coasts of California, Peru and Namibia show relative minima of PBL depth, while those of the western parts of the oceans show relative maxima. Altogehter, the patterns in Fig.

16a are very unrealistic. The incidence of startocumulus clouds tends to have relative maxima maxima in the western parts of the oceans in the fixed-sigma experiment while relative maxima appear in the eastern parts of the oceans in the CONTROL. The stratocumulus incidence in the low-pressure belt around Antartica is relatively well

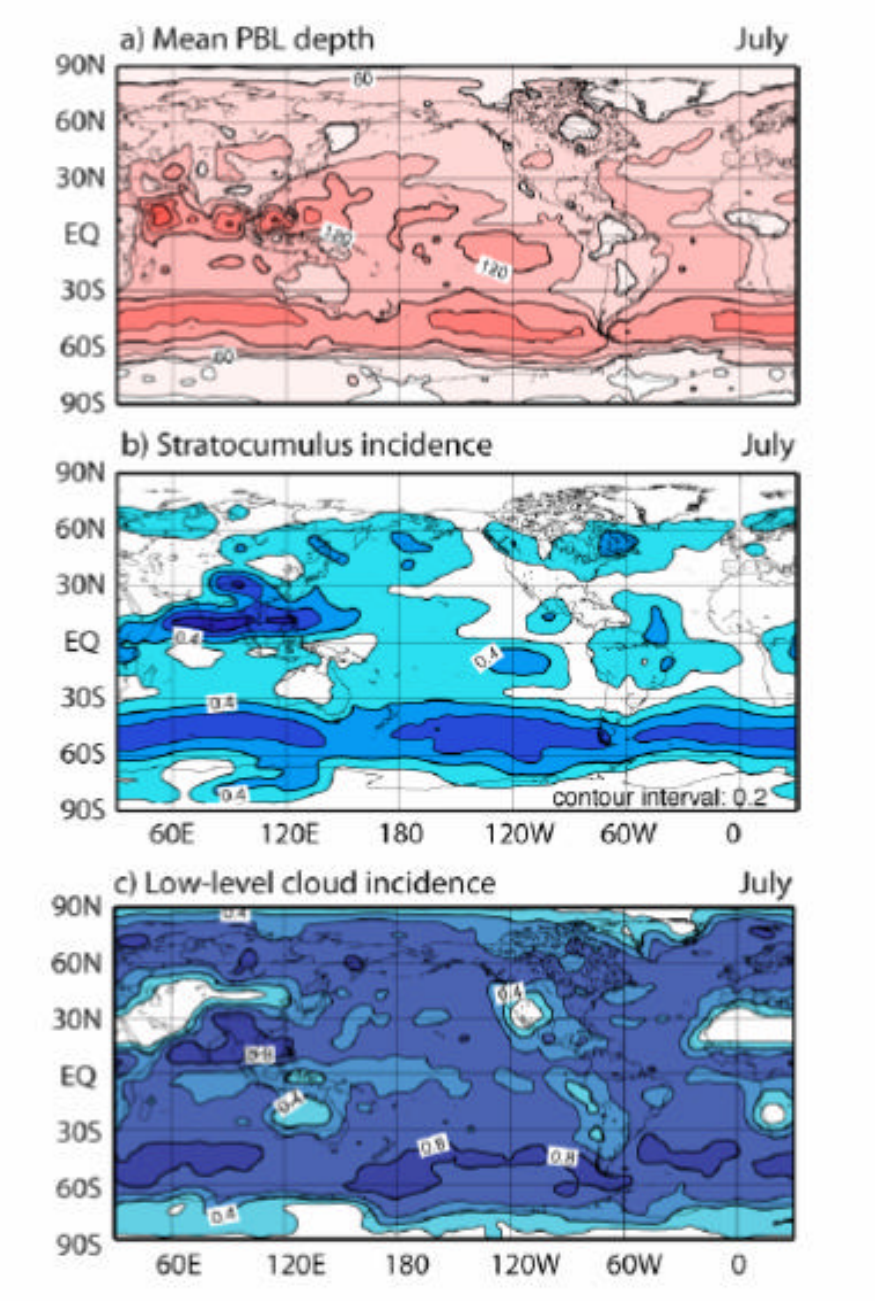

FIG. 16. (a) Monthly-mean PBL depth (hPa), (b) stratocumulus incidence (within the PBL) and (c) low-level cloud incidence (cloud incidence for the lowest 250 mb deep portion of the troposphere) for July from *fixed-sigma* simulation. See Fig. 4 for contour intervals.

simulated, but it has a more zonal pattern than in CONTROL. The low-level cloud incidence for July shown in Fig. 16c is overall unrealistically high almost everywhere, and tends to have relative minima in the usual marine startocumulus regions.

We interpret the differences between the results presented in Fig. 16 and the Control as the results of two main deficiencies in the fixed-sigma model. First, the formula that determines the PBL depth is diagnostic without considering the mass budget. Second, the processes a the cloud top that influence the turbulence are absent. According to the diagnostic equation that determines the PBL depth in the fixed-sigma model, the surface heat flux and the mean shear are the two main controllers of the PBL depth (the higher the upward flux is or the stronger the shear ism, the deeper the PBL is). In the fixed-sigma simulation, therefore, the PBL tends to be deeper in the areas with high SSTs. Only when the PBL is deep enough, the stratocumulus clouds can be maintained regardless of the processes associated with these clouds. In this case, it is not surprising that the important features of the marine PBL are poorly simulated in the fixed-sigma experiment.

7. Summary and Conclusions

In this paper, we present the basic features and an assesement of a newly developed PBL parameterization scheme implemented in the UCLA AGCM. The new scheme mantains many features of the previous PBL schemes of the UCLA AGCM (Suarez et al. 1983). These features can be summarized as follows: the depth of PBL is predicted through the mass budget for the PBL including the entrainment through its top, the cumulus mass flux and the vertically integrated horizontal mass flux convergence. Within the PBL a modified sigma coordinate is used, in which PBL and free atmosphere share a coordinate surface at the PBL top. The PBL top then becomes a material surface in the absence of entrainment (or detrainment) and cumulus mass flux. The new PBL scheme uses multiple layers as opposed to the single layer in the previous schemes. The vertically integrated turbulence kinetic energy (TKE) is predicted through a kinetic energy budget equation including the buoyancy and shear generation, dilution due to the PBL-top mass entrainment, and dissipation. The buoyancy generation includes the effects of the upward surface heat fluxes and radiative cooling at the cloud top (PBL-top and cloud top coincidence if PBL is cloudy). The PBL top entrainment is determined from a formulation that takes into account the effects on TKE and the radiative and evaporative cooling concentrated near the PBL top (Randall and Schubert 2004). The surface fluxes are determined from an aerodynamical formula, in which a combination of the square root of TKE and the grid-scale surface wind are used to represent the velocity scale. The turbulent fluxes within the PBL are determined through an approach considering the effects of both large convective and small diffusive eddies through bulk and K-closure

formulations, respectively. Using these fluxes, we explicitly predict the vertical profiles of the variables.

To illustrate the performance of the model with the new PBL parameterization, we carried out simulations in an uncoupled mode with prescribed SST and in a coupled mode using a near global MIT-OGCM. In this paper, we present the results from the uncoupled simulations. Monthly-mean fields of the simulated SLP, PBL depth, TKE, stratocumulus incidence and net solar radiation and latent heat fluxes at the surface are shown. These fields (except PBL height and TKE, for which observations are not available) match reasonably well to their observed counterparts. The distribution and seasonal variation of the stratocumulus incidence off the coasts of California, Peru and Namibia are realistic. A comparison of these results to the ones obtained by using the previous version of the PBL parameterization demonstrates an overall improvement in the simulations with the new parameterization. The simulated PBL profiles near the location of DYCOMS II field experiment demonstrate the same major features of the observed profiles. The composite diurnal cycles of various fields including PBL depth and precipitation over moist and semi-arid land points are also examined. Over semi-arid land point, the PBL reaches its maximum depth late afternoon just before sunset and crashes rapidly after sunset completing a cycle as observed in nature. Over moist land (a point chosen in the Amazon region), the diurnal cycle of precipitation shows precipitation peaks in the afternoon as observed.

Simulation of the formation and maintenance of the marine stratocumulus decks off the coasts of California, Peru and Namibia presents a real challenge for climate models. Success of the model generally depends on the formulation of the interactions

between radiation, turbulence and thermodynamics in the cloud-topped PBL. While the results presented in section 3 confirm the overall effectiveness and realism of the parameterized PBL processes with the new formulation, we additionally performed experiments to demonstrate the important role of these interactions in maintaining marine stratocumulus decks. We first eliminated the turbulence and radiative cooling interaction by setting the radiative cooling to zero in the buoyancy generation of TKE and in the entrainment formula. The results obtained from this experiment are very different from those of the control simulation. In the usual stratocumulus regions, the simulated cloud incidence is drastically reduced and the PBL becomes shallower and less turbulent compared to the Control. As an extension of this experiment, the radiative cooling effect is also removed from the potential temperature equation for the uppermost PBL layer. The simulation from this experiment virtually eliminates already infrequent stratocumulus incidence. These two experiments indicate that it is very difficult to maintain the clouds against the destructive effects of subsidence prevailing in these regions without properly simulating the cloud radiative cooling, turbulence and temperature interactions.

We also examine whether the AGCM would yield very different results if a PBL parameterization based on the formulation described by Holstlag and Boville (1993) is used. For this purpose, we modify the model to use the conventional sigma coordinate and determine the PBL height using the formula introduced by Treon and Marth (1986) and used by Holstlag and Boville (1993). The results are significantly worse than the control particularly for the stratocumulus incidence over the oceans. This comparison

also confirms the importance of cloud radiation-turbulence interaction processes in the PBL parameterization for realistic simulations of the startocumulus clouds.

In the coupled simulations, the SST field illustartes realistic equatorial SST gradients in both Pacific and Atlantic basins both in terms of annual means and interannual variability (such as ENSO-like anomalies in SST and the atmospheric circulation). We attribute a large part of this success to the merits of the PBL framework we used, particularly those involved in realistic representation of physical processes associated with startocumulus.

Two issues remain, one of wich is related to the transparency of the startocumulus clouds and the other related to the higher than observed liquid-water content in the startocumulus decks, as discussed in suvsections 3a and 3b, respectively. Both issues are complex and will be adresses in the future model revisions. The first step in this direction should be a detailed examination of simulated diurnal and seasonal variations of liquid water path with the current model. An observational analysis of diurnal and seasonal variations of liquid water path is presented by Wood et al. (2002).

One of the main weaknesses of existing AGCMs, including the model presented here, is poor representation of interactions between PBL and cumulus convection. The use of multiple layers within the PBL is the first step in our plan improving the simulation of these interactions. Another common weakness of AGCMs is in the simulation of the stably stratified PBL regimes (Holstlag 2003, Derbyshire 1990, and Beljaar and Holstlag 1991). An excellent discussion on this subject can be found in Marth (1999). Since the PBL reduces to a shallow layer for this condition, which is not well mixed, our new multi-layer framework should provide the necessary structure to treat the

stable shallow layer. Yet, a proper parameterization of physical processes involved in a stable PBL remains to be decided.

This paper presents a preliminary assessment of a new multi-layer framework for parameterizing PBL processes. So far, it is shown that the multi-layer framework is advantegeous for more realistic simulations of baroclinic activity compared to the single layer framework. Yet, much more work is needed to fully benefit form this potential, such as predicting TKE for each PBL layer and inclusion of a scheme to represent the cumulus roots. Betchold et al. (1992) presents a PBL parametrization, in which the vertical transport of TKE is formulated through a diffusive flux. However, TKE in our model is defined for large-eddies so that the transport may not be diffusive. It is one of our goals to improve this aspect of Betchold et al. model to implement in our model to predict TKE for each layer. To design a scheme for cumulus roots, we may take advantage of very high-resolution cloud resolving model simulations.

Acknowledgements. This research was supported by the Department of Energy, Grant DE-FG 02-04ER63848, Department of Energy Cooperative Agreement FG-02-01ER63163, Colorado State University Contract G-3816-3, NSF Grant ATM0071345, NOAA Grant NA030 AR4310095 and NASA CAN 21425/041. Professor David Randall assisted in discussions and making available mass entrainment formulation.

References

Albrecht, B. A., D. A. Randall, and S. Nicholls, 1988: Observations of marine stratocumulus clouds during FIRE. *Bull. Amer. Meteor. Soc*., **69**, 619-626.

Arakawa, A., 2004: The Cumulus Parameterization Problem: Past, Present, and Future**.** *J. Climate*, **17**, 2493–2525.

Arakawa, A., and V. R. Lamb, 1977: Computational design of the basic dynamical process of the UCLA general circulation model. *Methods in Computational Physics*, **17**, Academic Press, 173-265.

Arakawa, A., and W. H. Schubert, 1974: Interaction of a cumulus cloud ensemble with the large-scale environment, Part I. *J. Atmos. Sci.*, **31**, 674-701.

Bastable, H. G., W. J. Shuttleworth, R. L. G. Dallarosa, G. Fisch and C. A. Nobre, 1993: Observations of Climate, albedo, and surface radiation over cleared and undisturbed Amazonian forest. *J. Climatol.*, **13**, 783-796.

Bougeault, P., 1985: The diurnal cycle of the marine stratocumulus layer: A higher order model study. *J. Atmos. Sci*, **42**, 2826-2843.

Breidenthal, R. E. and M. B. Baker, 1985: Convection and entrainment across stratified interfaces. *J. Geophys. Res.,* **90D**, 13055-13062.

Breidenthal, R. E., 1992: Entrainment at thin stratified interfaces: The effects of Smith, Richardson and Reynolds numbers. *Phys. Fluids A,* **4**, 2141-2144.

Bretherton, C. S., 1992: A conceptual model of the stratocumulus-trade-cumulus transition in the subtropical oceans. *Proceedings, 11th International Conference on Clouds and Precipitation, Montreal, Canada, 374-377.*

Bretherton C. S., J. R. McCaa, and H. Grenier, 2004: A new parameterization for shallow cumulus convection and its application to marine subtropical cloud-topped boundary layers.Part I: description and 1D results. *Mon. Wea. Rev.*, **132**, 864-377.

Cazes Boezio, G. C. S. Konor, A. Arakaw, C. R. Mechoso and D. Menemenlis, 2005: Coupled simulations obtained with the UCLA AGCM with a new PBL parameterization and the MIT global OGCM. Proceedings of the 17h Conference on Climate Variability of the American Meteorological Society, Cambridge, Massachussets, May 2005.

Chen, C., and W. R. Cotton, 1987: The physics of the marine stratocumulus-capped mixed layer. *J. Atmos. Sci*., **44**, 2951-2977.

Da Silva, A. C. Young, and S. Levitus, 1994: Atlas of surface marine data, volume 1: Algorithms and procedures. *Tech. Rep. 6, U.S. Department of Commerce, NOAA, NESDIS, 1994.*

Deardorff, J. W., 1972: Parameterization of the planetary boundary layer use in general circulation models. *Mon. Wea. Rev*, 93-106. Deardorff, J. W., 1976: On the entrainment rate of a stratocumulus-capped mixed layer. *Quart. J. Roy. Meteor. Soc.*, **102**, 563-582.

Deardorff, J. W., 1980: Cloud top entrainment instability. *J. Atmos. Sci*, **37**, 329-350.

Del Genio, A., M.-S. Yao, W. Kovari, and K. K.-W. Lo; 1996: A prognostic cloud water parameterization for global climate models. *J. Climate,* **9**, 270-304.

Dorman, J. L., and P. J. Sellers, 1989: A global climatology of albedo, roughness length and stomatal resistance for atmospheric general circulation models as represented by the Simple Biosphere model (SiB). *J. Appl. Meteor.*, **28**, 833-855.

Grenier H. and C. S. Bretherton, 2001: A Moist PBL Parameterization for Large-Scale Models and Its Application to Subtropical Cloud-Topped Marine Boundary Layers. *Mon. Wea. Rev.*, **129**, 357-377.

Harshvardhan, R D., D. A. Randall and T. G. Corsetti, 1987: A fast radiation parameterization for atmospheric circulation models. *J. Geophys. Res*., **92**, 1009-1016.

Harshvardhan, R. D, D. A. Randall, T. G. Corsetti, and D. A. Dazlich, 1989: Earth radiation budget and cloudiness simulations with a general circulation model. *J. Atmos. Sci.*, **46,** 1922–1942.

Holtslag A. A. M. and B. A. Boville, 1993: Local versus nonlocal Boundary-layer diffusion ina global model. *J. Climate*, **6**, 1825-1842.

Holtslag A. A. M. E. I. F. Bruijn and H. L. Pan, 1990: A high resolution air mass transformation model for short-range weather forecasting. *Mon. Wea. Rev*., **118**, 1561-1575.

Kalnay. E. [and list of authors] 1996: The NCEP/NCAR 40-Year Reanalysis project. *Bull. Am. Met. Soc.*, **77**, 437-471.

Klein S. A. and D. L. Hartmann, 1993: The seasonal cycle of low stratiform clouds. *J. Climate*, **6**, 1587-1606.

Krueger, S. K., G. T. McLean, and Q. Fu, 1995a: Numerical simulation of the stratus-cumulus transition in the Subtropical marine boundary layer, Part I.: Boundary-layer structure. *J. Atmos. Sci*, **52**, 2839-2850.

Krueger, S. K., G. T. McLean, and Q. Fu, 1995b: Numerical simulation of the stratus-cumulus transition in the Subtropical marine boundary layer. Part II: Boundary-layer circulation *J. Atmos. Sci*, **52**, 2839-2850.

Konor C. S., and A. Arakawa, 2005b: Incorporation of moist processes and a PBL parameterization into the generalized vertical coordinate model. Techical Report 102, Department of Atmospheric Sciences, UCLA, 63 pp. Available from http://kiwi.atmos.colostate.edu/group/csk

Konor, C. S., G. Cazes Boezio, C. R. Mechoso and A. Arakawa, 2004: Evaluation of a new PBL paramaterization with emphasis in Surface Fluxes. Proceedings of the 13th Conference on Interactions of the Sea and Atmosphere of the American Meterological Society, (edited as CD), paper 2.11, Portland, Maine, 9-13 August 2004.

Lenschow D. H., [and list of authors] 1988: Dynamics and Chemistry of Marine Stratocumulus, (DYCOMS), *Bull. Am. Met. Soc.,* **69**, 1058-1067.

LeTreut, H., and Z.-H. Li, 1991: Sensitivity of an atmospheric general circulation model to prescribed SST changes: Feedback effects associated with the simulation of cloud optical properties. *Climate Dyn.,* **5**, 175-187.

Lilly, D. K., 1968: Models of cloud-topped mixed layers under a strong inversion. *Quart. J. Roy. Meteor. Soc.,* **94**, 292-309.

Lilly, D. K., 2002: Entrainment into mixed layers.Part I: a new closure. *J. Atmos. Sci*, **59**, 3353-3361.

Lin, X., D. A. Randall and L. D. Fowler, Diurnal variability of the hydrologic cycle and radiative fluxes: comparisons between observations and a GCM. *J. Climate*, **13**, 4159-4179.

Lock A. P., A. R. Brown, M. R. Bush, G. M. Martin and R. N. B. Smith, 2000: A new boundary layer mixing scheme. Part I: Scheme description and single-column Model. *Mon. Wea. Rev.*, **128**, 3187-3199.

Lock A. P., 1998: The Parameterization of entrainmet in cloudy boundary layers. *Quart. J. Roy. Meteor. Soc.*, **124**, 2729-2753.

Louis, J. F., 1979: A parametric model of vertical eddy fluxes in the atmosphere. *Boun.-Layer Meteor.*, **17**, 187-202.

Louis, J. F., M. Tiedke, and J. F. Geleyn, 1982: A short history of the PBL parameterization at ECMWF. *Proc. ECMWF Workshop on Boundary-Layer Parameterization*, ECMWF 59-79 [Available from ECMWF, Shinfield Park, Reading RG2 9AX U.K.]

Ma , C. -C., C. R. Mechoso, A. W. Robertson, and A. Arakawa, 1996: Peruvian Stratus Clouds and the Tropical Pacific Circulation: A Coupled Ocean-Atmosphere GCM Study, *J. Climate,* **9**, 1635-1645.

Machado, L. A. T., H. Laurent, and A. A. Lima (2002), Diurnal march of the convection observed during TRMM-WETAMC/LBA, *J. Geophys. Res.*, **107** (D20), 8064

Martin G. M., M. R. Bush, A. R. Brown, Lock A. P.and R. N. B. Smith, 2000: A new boundary layer mixing scheme. Part II: Tests in climate and mesoscale models. *Mon. Wea. Rev*., **128**, 3200-3217.

Mechoso, C.R., J-Y. Yu and A. Arakawa, 2000: A coupled GCM pilgrimage: from climate catastrophe to ENSO simulations. General Circulation Model Development: Past, Present and Future. Proceedings of a Symposium in Honor of Professor Akio Arakawa, D. A. Randall, Ed., Academic Press, pp. 539-575.

Mellor G. L. and T. Yamada, 1982: Development of a turbulence closure model for geophysical fluid problems. *Rev. Geophys. Space Phys.,* **20**, 851-875.

Moeng, C.-H., and A. Arakawa, 1980: A numerical study of a marine subtropical stratus cloud layer and its stability. *J. Atmos. Sci.*, **31**, 2661-2676.

Moeng, C.-H., 1986: Large-eddy simulation of a stratus-topped boundary layer. Part I: Structure and budgets. *J. Atmos. Sci*, **43**, 2886-2900.

Moeng, C.-H., 2000: Entrainment rate, cloud fraction and liquid water path of PBL stratocumulus clouds. *J. Atmos. Sci*, **57**, 3627-3643.

Moeng, C.-H., and Co-authors, 1996: Simulation of a stratocumulus-topped planetary boundary layer. Intercomparison among different numerical codes. *Bull. Amer. Meteor. Soc*., **77**, 261-278.

Nicholls, S., 1984: The dynamics of stratocumulus: Aircraft observations and comparisons with a mixed layer model. *Quart. J. Roy. Meteor. Soc.,* **110**, 783-820.

Pan, D. M. and D. A. Randall, 1998: A cumulus parameterization with a prognostic clossure. *Quart. J. Roy. Meteor. Soc.,* **124**, 949-981.

Randall, D. A., 1976: The interaction of the planetary boundary layer with large scale circulations. Ph. D. Thesis, The University of California. Los Angeles, 247 pp.

Randall, D. A., 1980a: Conditional instability of the first kind upside-down. *J. Atmos. Sci*., **37**, 125-130.

Randall, D. A., 1980b: Entrainment into a stratocumulus layer with disturbed radiative cooling. *J. Atmos. Sci*., **37**, 148-159.

Randall, D. A., and M. J. Suarez, 1984: On the dynamics of stratocumulus formation and dissipation, *J. Atmos. Sci*., **41**, 3052-3057.

Randall, D. A., R. D. Harshvardhan, D. A. Dazlich and T. G. Corsetti, 1989: Interactions among Radiation, Convective, and Large-Scale Dynamics in a General Circulation Model, *J. Atmos. Sci*, **46**, 1943-1970.

Randall D. A., and W. H. Schubert, 2004: Dreams of a stratocumulus sleeper.` In Atmospheric Turbulence and Mesoscale Meteorology, Scientific Research Inspired by Doug Lily, E. Fedorovich, R. Rotuno and B. Stevens (eds.), Cambridge University Press, 95-114.

Rayner, N. A., C. K. Folland, D. E. Parker, and E. B. Horton, 1995:A new global sea-ice and sea surface temperature (GISST) data set for 1903–1994 for forcing climate models. Hadley Centre Internal Note 69, U.K. Met. Office, 14 pp.

Schubert, W. H., 1976: Experiments with Lilly's cloud-topped model. *J. Atmos. Sci*, **33**, 436-446.

Schubert, W. H., J. S. Wakefield, E. J. Steiner, and S. K. Cox, 1979: Marine stratocumulus convection.Part I: Governing equations and horizontally homogeneous solutions. *J. Atmos. Sci*, **36**, 1286-1307.

Siens, S. T., C. S. Bretherton, M. B. Baker S. Shy and R. E. Breidenthal, 1990: Buoyancy reversal and cloud top instability. *Quart. J. Roy. Meteor. Soc.*, **116**, 705-739.

Slingo, A. S., Nicholls, and J. Schmetz, 1982: Aircraft observations of marine stratocumulus during JASIN, *Quart. J. Roy. Meteor. Soc.*, **108**, 833-856.

Stages, S. A., and Businger, J. A., 1981: A model for entrainment into a cloud-topped marine boundary. Part I: Model description and application to a cold-air outbreak episode, *J. Atmos. Sci*, **38**, 2213-2229.

Stevens B., W. R. Cotton, G. Feingold and C. H. Moeng, 1998: Large-eddy simulations of strongly precipitating, shallow, stratocumulus-toped boundary layers. 2002: Entrainment in stratocumulus topped mixed layers, *J.Atmos. Sci.,* **55**, 3616-3638.

Stevens B., 2002: Entrainment in stratocumulus topped mixed layers, *Quart. J. Roy. Meteor. Soc.,* **119**, 1-26.

Stevens B., [and list of authors] 2003: Dynamics and Chemistry of Marine Stratocumulus, DYCOMS-II, *Bull. Am. Met. Soc.,* **84**, 1579-593.

Smith, R. N. B., 1990: a Scheme for predicting layer clouds and their water content in a general circulation model. *Quart. J. Roy. Meteor. Soc.,* **116**, 435-460.

Suarez, M. J., A. Arakawa, and D. A. Randall, 1983: The parameterization of the planetary boundary layer in the UCLA general circulation model: Formulation and results. *Mon. Wea. Rev*., **111**, 2224-2243.

Sundqvist, H., 1978: A parameterization scheme for non-convective condensation including prediction of cloud water content, *Quart. J. Roy. Meteor. Soc.*, **104**, 677-690.

Terra R. 2004: PBL stratiform cloud inhomogeneities thermally induced by the orography: a parameterization for climate models. *J. Atmos. Sci.*, **61**, 644–663

Tokioka, T., K. Yamazaki, I. Yagai, and A. Kitoh, 1984: A description of the Meteorological Research Institute atmospheric general circulation model (MRI GCM-I). MRI Tech. Report No. 13, Meteorological Research Institute, Ibaraki-ken, Japan, 249 pp.

Troen, I. And L. Marth, 1986: A simple model of the atmospheric boundary layer: Sensitivity to surface evaporation. *Boun.-Layer Meteor.,* **37**, 129-148.

Turton, J. D. and S. Nicholls, 1987: A study of the diurnal variations of stratocumulus using a multiple mixed layer model. *Quart. J. Roy. Meteor. Soc.,* **113**, 969-10.

APPENDIX A

Prognostic equation for vertically averaged turbulent kinetic energy.

From equation 1.5,

$$\frac{\partial e}{\partial t} = -w\frac{\partial e}{\partial z} + g\frac{\overline{w'q_v'}}{q_v} + \overline{w'u'}\frac{\partial u}{\partial z} + \overline{w'v'}\frac{\partial v}{\partial z} - \frac{1}{r}\frac{\partial}{\partial z}\left(r\overline{w'e'} + \overline{w'p'}\right) - e$$

we consider $\frac{\overline{w'q_v'}}{q_v} = \frac{\overline{w'T_v'}}{T_v} = \frac{\overline{w'c_pT_v'}}{c_pT_v} = \frac{\overline{w'c_pT_v'}}{c_p\, p/Rr} = k\frac{r\overline{w's_v'}}{p}$ and we multiply equation above by ρ,

$$r\frac{\partial e}{\partial t} = -rw\frac{\partial e}{\partial z} + k\frac{r\overline{w's_v'}}{p}rg + r\overline{w'u'}\frac{\partial u}{\partial z} + r\overline{w'v'}\frac{\partial v}{\partial z} - \frac{\partial}{\partial z}\left(r\overline{w'e'} + \overline{w'p'}\right) - re$$

using mass conservation equation,

$$\frac{\partial(re)}{\partial t} = -\frac{\partial(rwe)}{\partial z} + k\frac{r\overline{w's_v'}}{p}rg + r\overline{w'u'}\frac{\partial u}{\partial z} + r\overline{w'v'}\frac{\partial v}{\partial z} - \frac{\partial}{\partial z}\left(r\overline{w'e'} + \overline{w'p'}\right) - re$$

We define vertical mass weighted average of e through the PBL as e_{PBL},

$$e_{PBL} \equiv \frac{g}{p_{PBL}}\int_{z_S}^{z_B} re\,dz$$

We then develop the predicting equation for e_{PBL} though vertical average of prediction equation for e given above. We compute vertical integral from z_S to z_B,

$$\int_{z_S}^{z_B}\frac{\partial(re)}{\partial t}dz =$$

$$-\int_{z_S}^{z_B}\frac{\partial(rwe)}{\partial z}dz + k\int_{z_S}^{z_B}\frac{r\overline{w's_v'}}{p}rg\,dz + \int_{z_S}^{z_B}\left(r\overline{w'u'}\frac{\partial u}{\partial z} + r\overline{w'v'}\frac{\partial v}{\partial z}\right)dz - \int_{z_S}^{z_B}\frac{\partial}{\partial z}\left(r\overline{w'e'} + \overline{w'p'}\right)dz - \int_{z_S}^{z_B} re\,dz$$

Through the definition of ePBL we have

$$\int_{z_S}^{z_B} \frac{\partial(\rho e)}{\partial t} dz = \frac{\partial}{\partial t} \int_{z_S}^{z_B} \rho e dz = \frac{\partial(\pi_{PBL} e_{PBL})}{\partial t}$$

and considering e = 0 and w' = 0 at z_S and z_B, and considering the definition of e_{PBL}, we have

$$\frac{1}{g} \frac{\partial(p_{PBL} e)}{\partial t} = k \int_{z_S}^{z_B} \frac{r \overline{w's'_v}}{p} r g \, dz + \int_{z_S}^{z_B} \left(r \overline{w'u'} \frac{\partial u}{\partial z} + r \overline{w'v'} \frac{\partial v}{\partial z} \right) dz - \int_{z_S}^{z_B} r e \, dz$$

using hydrostatic relation for variable change in the vertical integral of buoyancy flux (first term at the right hand side), we have

$$\frac{\partial(p_{PBL} e)}{\partial t} = k g \int_{p_B}^{p_S} \frac{r \overline{w's'_v}}{p} dp + g \int_{z_s}^{z_B} \left(r \overline{w'u'} \frac{\partial u}{\partial z} + r \overline{w'v'} \frac{\partial v}{\partial z} \right) dz - g \int_{z_S}^{z_B} r e \, dz,$$

and from mass balance for the whole PBL column (equation xxx) we conclude

$$\frac{\partial e_{PBL}}{\partial t} = \frac{g}{p_{PBL}} \left[k \int_{p_B}^{p_S} \frac{r \overline{w's'_v}}{p} dp + \int_{z_S}^{z_B} \left(r \overline{w'u'} \frac{\partial u}{\partial z} + r \overline{w'v'} \frac{\partial v}{\partial z} \right) dz - \int_{z_S}^{z_B} r e \, dz \right] + \frac{e_{PBL}}{p_{PBL}} \int_{p_B}^{p_S} \frac{\nabla . (p_{PBL} \vec{r} v)}{p_{PBL}} dp - \frac{gE}{p_{PBL}} = 0$$

which is our prognostic equation for e_{PBL}.

Appendix B

Small eddies diffusion coefficient K

The diffusion coefficient for a variable ψ is given by

$$K_\psi = \alpha k w_\psi z\left(1-\frac{z}{(\delta z)_{PBL}}\right)^2 \qquad (A.1)$$

where ? is a scale factor, k is the Von Karman constant, w_ψ is a scale velocity, z is the height above the Earth's surface, and $(? z)_{PBL}$ is the PBL's total thickness. Note that w_h and $(? z)_{PBL}$ are non-local parameters. In the case of a cloud topped PBL, $K_?$? is given by (A.1) in the sub-cloud layer, while it has a constant and large value (currently taken as 20 m^2/s) in the cloud layer.

For the computation of w_h, we examine whether the PBL is convectively unstable or stable in terms of the sign of the turbulent flux of $? _v$ at the Earth's surface.

Unstable conditions:

If $z < 0.1(? z)_{PBL}$ the scale velocity for moist static energy and water mixing ratio is given by,

$$w_h = \frac{u_*}{\phi_h} \;;\; \phi_h \equiv \left(1-15\frac{z}{L}\right)^{-1/2}, \qquad (A.2)$$

where u* is the friction velocity, $u^*=(F_{vs}/? _{PBL})^{1/2}$. For momentum (u and v) the corresponding expression is ,

$$w_m = \frac{u_*}{\phi_m} \;;\; \phi_m \equiv \left(1-15\frac{z}{L}\right)^{-1/3}. \qquad (A.3)$$

If $z > 0.1(? z)_{PBL,}$

$$\left.\begin{aligned} w_h &= \sqrt{e_{PBL}} \\ w_m &= Pr\sqrt{e_{PBL}} \end{aligned}\right\}, \qquad \text{(A.4)}$$

where Pr is the Prantl number, which is a function of the ratio of the buoyancy production (B) to shear production (S) of TKE given by equations (8.4) and (8.5) of Konor and Arakawa (2005a). This function is 1.0 for B/S=0 and 0.6 for B/S ≥10.0, in between we currently interpolate linearly.

Stable conditions:

If $z < 0.1(?\ z)_{PBL;}$

$$w_h = \frac{u_*}{\phi_h} \ ;\ \phi_h \equiv \min\left(1+5\frac{z}{L}\ ,\ 5+\frac{z}{L}\right) \qquad \text{(A.5)}$$

and $w_m = w_h$.

If $z > 0.1(?\ z)_{PBL}$.

$$w_h = \beta\sqrt{e_{PBL}} \qquad \text{(A.6)}$$

with

$$\beta \equiv \min\left(1\ ,\ \frac{u_*}{z_a\phi_h\sqrt{e_{PBL}}}\right)\ ,\ \text{and}\ \ \phi_h \equiv \min\left(1+5\frac{0.1(\delta z)_{PBL}}{L}\ ,\ 5+1\frac{0.1(\delta z)_{PBL}}{L}\right) \qquad \text{(A.7)}$$

and again $w_m = w_h$.

APPENDIX C

Entrainment Closure

The formulation discussed here was first implemented by Krasner (1993) in a one-dimensional model and have been recently published by Randall and Schubert (2004). Here we repeat the discussion for convenience.

a. Dry clear PBL

The entrainment parameterization follows the ideas of Breidenthal and Baker (1985), Siems et al. (1990) and Breidenthal (1989). The entrainment rate can be given by

$$E = \frac{b_1 r_B \sqrt{e_{PBL}}}{1 + b_2 R_{i\Delta}} . \tag{C.1}$$

Here b_1 and b_2 are assumed to be constants, and the relevant Richardson number is

$$R_{i\Delta} \equiv \frac{g(\Delta q_v)_B (dz)_{PBL}}{q_B e_{PBL}} . \tag{C.2}$$

To determine b_1 and b_2, we first consider the strong inversion (or highly stable) case. In this case $b_2 R_{i\Delta} >> 1$, and (C.1) becomes

$$E = \frac{b_1 r_B \sqrt{e_{PBL}}}{b_2 R_{i\Delta}} . \tag{C.3}$$

Now we require that (C.3) satisfy

$$-\left(F_{q_v}\right)_B = k\left(F_{q_v}\right)_S , \tag{C.4}$$

where $k \approx 0.2$, under the condition that the entrainment, buoyancy generation and dissipation effects are in a balance yielding no TKE change. Then, using (4.3), we can write

$$\left[\frac{\left(F_{q_v}\right)_S + \left(F_{q_v}\right)_B}{2}\right]\frac{g(dz)_{PBL}}{q_S} = C r_{PBL}\left(e_{PBL}\right)^{3/2}, \tag{C.5}$$

Here $C \approx 1$ (according to Moeng and Sullivan, 1994). Using (C.4) in (C.5), we find that

$$\left(\frac{1-k}{2}\right)\left(F_{q_v}\right)_S \frac{g(dz)_{PBL}}{q_S} = C r_{PBL}\left(e_{PBL}\right)^{3/2}. \tag{C.6}$$

Now using

$$\left(F_{q_v}\right)_B = -E\left(\Delta q_v\right)_B \tag{C.7}$$

in (C.4), we obtain

$$\left(F_{q_v}\right)_S = \frac{E\left(\Delta q_v\right)_B}{k}. \tag{C.8}$$

Using (C.8) in (C.6) and after some arrangement, we obtain an alternative equation that determines the entrainment rate as

$$E = \left(\frac{2kC}{1-k}\right)\left(\frac{r_{PBL}\sqrt{e_{PBL}}}{\frac{g\left(\Delta q_v\right)_B (dz)_{PBL}}{q_S e_{PBL}}}\right). \tag{C.9}$$

A comparison of (C.9) to (C.1) ignoring the difference between q_S and q_B yields that

$$\frac{b_1}{b_2} \cong \frac{2kC}{1-k}. \tag{C.10}$$

Since C=1 and k=0.2, we find that $b_1/b_2 \approx 0.5$. Now we consider the neutral case, for which

$$R_{i\Delta} = 0 \tag{C.11}$$

and, therefore,

$$\left(F_{q_v}\right)_B = 0. \tag{C.12}$$

For this case, (C.1) should be consistent with

$$E = D\rho_B w^*, \tag{C.13}$$

where $D \approx 0.2$ and w^* is the convective velocity scale of Deardorff (1970) in the present notation approximately given by

$$w^* = \left[\frac{g\left(F_{q_v}\right)_S (dz)_{PBL}}{(\rho q)_S}\right]^{1/3} \tag{C.14}$$

The relation (C.14) is obtained through LES by Deardorff (1974). In this neutral (no-inversion) case, (C.1) becomes

$$E = b_1 \rho_B \sqrt{e_{PBL}}\ . \tag{C.15}$$

A comparison of (C.15) to (C.13) yields that

$$w^* \cong \frac{b_1}{D}\sqrt{e_{PBL}} \tag{C.16}$$

Since $\left(F_{q_v}\right)_B = 0$ for the neutral case, (C.5) becomes

$$\left(F_{q_v}\right)_S \frac{g(dz)_{PBL}}{r_{PBL} q_S} = 2C\left(e_{PBL}\right)^{3/2}. \tag{C.17}$$

Taking advantage of the similarity between (C.17) and (C.14) by ignoring minor differences, we find

$$w^* \cong (2C)^{1/3}\sqrt{e_{PBL}}\,. \tag{C.18}$$

Comparing (C.16) to (C.18), we obtain b_1 as

$$b_1 \cong D(2C)^{1/3}. \tag{C.20}$$

Since $D \approx 0.2$ and $C \approx 1$, $b_1 \approx 0.25$, so that, $b_2 \approx 0.5$.

b. Smoke-cloud topped PBL

This case considers a PBL topped with smoke cloud, with radiative cooling at its top, but no phase changes. The presence of radiative cooling can affect the entrainment rate through two processes: *i*) it can increase the TKE and ii) it can cool the entraining air, thus

making the inversion (PBL-top jump) appear to be weaker that it really is. Through (C.1) and (C.2) the former process is already included in our formulation. Yet the latter needs to be incorporated. The method we use is based on a modification of the inversion strength to reflect the effect of reduced stability due to radiative cooling in the expression for Richardson number given by (C.2).

To do that, we employ a "mass flux" model. According to Randall et al. (1992), in a situation schematically demonstrated in Fig. D1, we can write

$$\left(y_d\right)_{B^-} = c_E \bar{y}_{B^+} + \left(1 - c_E\right)\bar{y}_{B^-} + \frac{c_E}{E}\int_{z_{B^-}}^{z_{B^+}} \bar{S}_y \, dz \,, \tag{C.20}$$

Here y is an intensive arbitrary quantity, subscript d denotes a "downdraft" property, c_E is a "mixing parameter" given by

$$c_E = \frac{s_B E}{M_B} \,, \tag{C.21}$$

where bar denotes average across updrafts and downdrafts, σ_B is the fractional area covered by updraft, M_B is a convective mass flux, and $\bar{S}_y$ is the source or sink of y within the inversion (transition) layer.

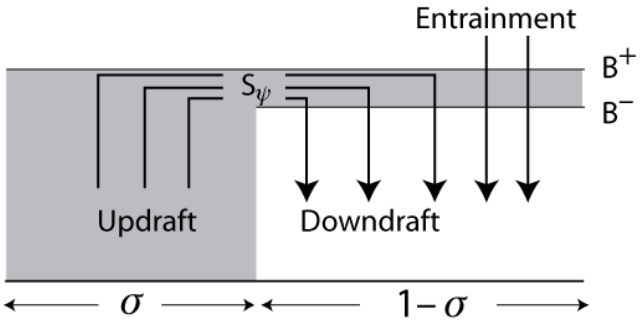

Fig. D1.

If we choose $y \equiv h$, then $\int_{z_{B^-}}^{z_{B+}} \bar{S}_y \, dz = -(\Delta R)_B$. Note that $(\Delta R)_B > 0$ for radiative cooling. For this case, (C.20) becomes

$$(h_d)_{B^-} = c_E \bar{h}_{B^+} + (1 - c_E)\bar{h}_{B^-} - \frac{c_E}{E}(\Delta \bar{R})_B . \tag{C.22}$$

Now we find the expression for the "effective" mean moist static energy at B+ level $(\bar{h}_{B^+})_{eff}$ form

$$c_E \bar{h}_{B^+} + (1 - c_E)\bar{h}_{B^-} - \frac{c_E}{E}(\Delta \bar{R})_B = c_E (\bar{h}_{B^+})_{eff} + (1 - c_E)\bar{h}_{B^-} , \tag{C.23}$$

which immediately becomes

$$(\Delta \bar{h})_{eff} = \bar{h}_{B^+} - \frac{(\Delta \bar{R})_B}{E} . \tag{C.24}$$

In (C.24), we define $(\Delta \bar{h})_{eff} \equiv (\bar{h}_{B^+})_{eff} - \bar{h}_{B^-}$. Now we modify the definition of the Richardson number (C.2). We first write

$$(\Delta \bar{q}_v)_{eff} = (\Delta \bar{q}_v)_B - \left(\frac{1}{\Pi_B}\right)\frac{(\Delta \bar{R})_B}{E} \tag{C.25}$$

and, then, the Richardson number using (C.25) as

$$\left(R_{i\Delta}\right)_{eff} \equiv \frac{g\left(dz\right)_{PBL}}{\bar{q}_{B^-} e_{PBL}} \left[\left(\Delta \bar{q}_v\right)_B - \left(\frac{1}{\Pi_B}\right) \frac{\left(\Delta \bar{R}\right)_B}{E} \right]. \tag{C.26}$$

Using (C.26) in (C.1), we obtain

$$E = \frac{b_1 r_{B^-} \sqrt{e_{PBL}}}{1 + b_2 \frac{g\left(dz\right)_{PBL}}{\bar{q}_{B^-} e_{PBL}} \left[\left(\Delta \bar{q}_v\right)_B - \left(\frac{1}{\Pi_B}\right) \frac{\left(\Delta \bar{R}\right)_B}{E} \right]}. \tag{C.27}$$

By rearranging the terms in (C.27), we obtained the equation that determines the entrainment rate for a PBL topped by smoke cloud as

$$E = \frac{b_1 r_{B^-} \sqrt{e_{PBL}} + b_2 \frac{g\left(dz\right)_{PBL}}{e_{PBL} \Pi_B \bar{q}_{B^-}} \left(\Delta \bar{R}\right)_B}{1 + b_2 \frac{g\left(dz\right)_{PBL} \left(\Delta \bar{q}_v\right)_B}{\bar{q}_{B^-} e_{PBL}}} \tag{C.28}$$

or

$$E = \frac{b_1 r_{B^-} \sqrt{e_{PBL}} + b_2 \frac{g\left(dz\right)_{PBL}}{e_{PBL} \Pi_B \bar{q}_{B^-}} \left(\Delta \bar{R}\right)_B}{1 + b_2 R_{i\Delta}} \tag{C.29}$$

Under the strong inversion, neglecting “1” in the denominator of (C.28), the entrainment equation (C.29) becomes

$$E = \left(\frac{b_1}{b_2} r_{B^-} \frac{(e_{PBL})^{3/2}}{g(dz)_{PBL}} + \frac{(\Delta \bar{R})_B}{\bar{q}_{B^-} \Pi_B} \right) \frac{\bar{q}_B}{(\Delta \bar{q}_v)_B}. \tag{C.30}$$

c. Water-cloud topped PBL

Now we write

$$(r_d)_{B^-} = c_E \bar{r}_{B^+} + (1 - c_E) \bar{r}_{B^-}. \tag{C.31}$$

Since the air is saturated, we can write

$$(s_{vd})_{B^-} - (\bar{s}_v)_{B^-} = b_{B^-} \left[(h_d)_{B^-} - \bar{h}_{B^-} \right] - e_{B^-} L \left[(r_d)_{B^-} - \bar{r}_{B^-} \right], \tag{C.32}$$

where $e_B \equiv \Pi_B \bar{q}_B / L$. Using (C.22) in (C.32), we obtain

$$(s_{vd})_{B^-} - (\bar{s}_v)_{B^-} = b_{B^-} \left[c_E \bar{h}_{B^+} + (1 - c_E) \bar{h}_{B^-} - \frac{c_E}{E} (\Delta \bar{R})_B - \bar{h}_{B^-} \right] - e_{B^-} L \left[c_E \bar{r}_{B^+} + (1 - c_E) \bar{r}_{B^-} - \bar{r}_{B^-} \right] \tag{C.33}$$

After some arrangements, (C.33) becomes

$$(s_{vd})_{B^-} - (\bar{s}_v)_{B^-} = c_E \left[b_{B^-} (\Delta \bar{h})_B - e_{B^-} L (\Delta \bar{r})_B - b_{B^-} \frac{(\Delta \bar{R})_B}{E} \right]. \tag{C.34}$$

Now let us define $b_{B^-}\left(\Delta\bar{h}\right)_B - e_{B^-}L\left(\Delta\bar{r}\right)_B \equiv \left(\Delta\bar{s}_v\right)_B - \left(\Delta\bar{s}_v\right)_{crit}$ following Randall (1980) and rewrite the right hand side of (C.34) as

$$c_E\left[b_{B^-}\left(\Delta\bar{h}\right)_B - e_{B^-}L\left(\Delta\bar{r}\right)_B - b_{B^-}\frac{\left(\Delta\bar{R}\right)_B}{E}\right] \equiv c_E\left\{\left[\left(\Delta\bar{s}_v\right)_B - \left(\Delta\bar{s}_v\right)_{crit}\right] - b_{B^-}\frac{\left(\Delta\bar{R}\right)_B}{E}\right\}. \qquad \text{(C.35)}$$

Phase changes and radiative cooling make the inversion seem weaker than it really is. We define $\left(\bar{s}_{vB^+}\right)_{eff}$ by

$$\left(s_{vd}\right)_{B^-} = c_E\left(\bar{s}_{vB^+}\right)_{eff} + \left(1 - c_E\right)\left(\bar{s}_v\right)_{B^-}, \qquad \text{(C.36)}$$

so that

$$\left(s_{vd}\right)_B - \left(\bar{s}_v\right)_B = c_E\left(\Delta\bar{s}_v\right)_{eff}, \qquad \text{(C.37)}$$

where $\left(\Delta\bar{s}_v\right)_{eff} = \left(\bar{s}_{vB^+}\right)_{eff} - \left(\bar{s}_v\right)_{B^-}$. A comparison of (C.35) to (C.37) shows that

$$\left(\Delta\bar{s}_v\right)_{eff} = \left[\left(\Delta\bar{s}_v\right)_B - \left(\Delta\bar{s}_v\right)_{crit}\right] - b_{B^-}\frac{\left(\Delta\bar{R}\right)_B}{E}. \qquad \text{(C.38)}$$

To obtain the equation that determines the entrainment rate for this case, we first write the Richardson equation (C.2) in terms of the virtual static energy as

$$R_{i\Delta} \equiv \frac{g\left(\Delta\bar{s}_v\right)_B\left(dz\right)_{PBL}}{\Pi_B\bar{q}_{B^-}e_{PBL}}. \qquad \text{(C.39)}$$

Then, replacing $\left(\Delta\bar{s}_v\right)_B$ by $\left(\Delta\bar{s}_v\right)_{eff}$ in (C.39) and substituting the result into (C.1), we find

$$E = \frac{b_1 r_{B^-}\sqrt{e_{PBL}}}{1 + b_2 \dfrac{g(dz)_{PBL}}{\Pi_B \bar{q}_{B^-} e_{PBL}} \left\{ \left[\left(\Delta\bar{s}_v\right)_B - \left(\Delta\bar{s}_v\right)_{crit} \right] - b_{B^-} \dfrac{\left(\Delta\bar{R}\right)_B}{E} \right\}} \tag{C.40}$$

After some arrangements, we obtain the equation that determines the entrainment rate for a water-cloud topped PBL as

$$E = \frac{b_1 r_{B^-}\sqrt{e_{PBL}} + b_2 \dfrac{g(dz)_{PBL}}{\Pi_B \bar{q}_{B^-} e_{PBL}} b_{B^-} \left(\Delta\bar{R}\right)_B}{1 + b_2 \dfrac{g(dz)_{PBL}}{\Pi_B \bar{q}_{B^-} e_{PBL}} \left[\left(\Delta\bar{s}_v\right)_B - \left(\Delta\bar{s}_v\right)_{crit} \right]} . \tag{C.41}$$